Neurobiology of Aging 90 (2020) 60–74

Contents lists available at ScienceDirect

Neurobiology of Aging

journal homepage: www.elsevier.com/locate/neuaging

A high-sucrose diet aggravates Alzheimer's disease pathology, attenuates hypothalamic leptin signaling, and impairs food-anticipatory activity in APPswe/PS1dE9 mice

Skye Hsin-Hsien Yeh [a,1], Feng-Shiun Shie [b,1], Hui-Kang Liu [c,d], Heng-Hsiang Yao [e], Pei-Chen Kao [b], Yi-Heng Lee [e,f], Li-Min Chen [e], Shu-Meng Hsu [b,e], Li-Jung Chao [a], Kuan-Wei Wu [g], Young-Ji Shiao [c,d,g,*], Huey-Jen Tsay [e,**]

[a] Brain Research Center, National Yang-Ming University, Taipei, Taiwan, R.O.C.
[b] Center for Neuropsychiatric Research, National Health Research Institutes, Taiwan, Miaoli, Taiwan, R.O.C.
[c] National Research Institute of Chinese Medicine, Ministry of Health and Welfare, Taipei, Taiwan
[d] Ph.D. Program in Clinical Drug Development of Chinese Herbal Medicine, Taipei Medical University, Taipei, Taiwan, R.O.C.
[e] Institute of Neuroscience, School of Life Science, National Yang-Ming University, Taipei, Taiwan, R.O.C.
[f] Taiwan International Graduate Program in Interdisciplinary Neuroscience, National Yang-Ming University and Academia Sinica, Taipei, Taiwan, R.O.C.
[g] Institute of Biopharmaceutical Science, National Yang-Ming University, Taipei, Taiwan, R.O.C.

ARTICLE INFO

Article history:
Received 3 April 2019
Received in revised form 19 November 2019
Accepted 22 November 2019
Available online 27 November 2019

Keywords:
High-sucrose diet
Alzheimer's disease
amyloid-β
Hypothalamus
Leptin
Signal transducer and activator of transcription 3, STAT3

ABSTRACT

High-fat and high-sugar diets contribute to the prevalence of type 2 diabetes and Alzheimer's disease (AD). Although the impact of high-fat diets on AD pathogenesis has been established, the effect of high-sucrose diets (HSDs) on AD pathogenesis remains unclear. This study sought to determine the impact of HSDs on AD-related pathologies. Male APPswe/PS1dE9 (APP/PS1) transgenic and wild-type mice were provided with HSD and their cognitive and hypothalamus-related noncognitive parameters, including feeding behaviors and glycemic regulation, were compared. HSD-fed APP/PS1 mice showed increased neuroinflammation, as well as increased cortical and serum levels of amyloid-β. HSD-fed APP/PS1 mice showed aggravated obesity, hyperinsulinemia, insulin resistance, and leptin resistance, but there was no induction of hyperphagia or hyperleptinemia. Leptin-induced phosphorylation of signal transducer and activator of transcription 3 in the dorsomedial and ventromedial hypothalamus was reduced in HSD-fed APP/PS1 mice, which might be associated with attenuated food-anticipatory activity, glycemic dysregulation, and AD-related noncognitive symptoms. Our study demonstrates that HSD aggravates metabolic stresses, increases AD-related pathologies, and attenuates hypothalamic leptin signaling in APP/PS1 mice.

1. Introduction

Alzheimer's disease (AD) is an age-related neurodegenerative disease. Over 95% of AD cases are sporadic with unknown etiology (Masters et al., 2015). Extracellular amyloid-β (Aβ) depositions and neurofibrillary tangles are the neuropathological hallmarks of AD. Aβ accumulation induces neurotoxicity, neuroinflammation, and synaptic dysfunction, all of which play pivotal roles in AD pathophysiology (Heneka et al., 2015; Sakono and Zako, 2010).

Systemic insulin signaling plays a role in nutrient metabolism. Insulin may preserve brain function and structure in the central nervous system (CNS). Furthermore, insulin resistance may be a pathogenic factor for AD (De Felice et al., 2014; de la Monte, 2017; Spielman et al., 2014). This line of inquiry is currently under intensive investigation (Frazier et al., 2019; Lyra e Silva et al., 2019). Inflammation and impaired insulin signaling, which is associated with type 2 diabetes, is also likely to promote AD pathology (Baglietto-Vargas et al., 2016; De Felice et al., 2014). Disruptions to brain glucose utilization and metabolic hormones are considered to be key elements in AD pathophysiology (Bonda et al., 2014).

* Corresponding author at: National Research Institute of Chinese Medicine, Ministry of Health and Welfare, LiNung Street, Peitou, Taipei 112, Taiwan. Tel.: 011886282019994163; fax: 0118860228264266.
** Corresponding author at: Institute of Neuroscience, School of Life Science, National Yang-Ming University, Taipei 112, Taiwan. Tel.: 011886 0228267154; fax: 0118860228200259.
E-mail addresses: yshiao@nricm.edu.tw (Y.-J. Shiao), hjtsay@ym.edu.tw (H.-J. Tsay).
[1] Yeh and Shie contributed equally to this manuscript.

https://doi.org/10.1016/j.neurobiolaging.2019.11.018

Leptin secreted by white adipose tissue acts on the hypothalamus and brainstem to regulate energy homeostasis (Caron et al., 2018). Leptin receptors are abundantly expressed in the hypothalamic appetite control nuclei, including the arcuate nucleus (ARC), the dorsomedial hypothalamus (DMH), and the ventromedial hypothalamus (VMH) (van Swieten et al., 2014; Zhang et al., 2015). Leptin induces phosphorylation of signal transducer and activator of transcription 3 (STAT3). Phosphorylated STAT3 (pSTAT3) upregulates pro-opiomelanocortin (*POMC*) gene and downregulates Agouti-related protein (*AgRP*), and neuropeptide Y (*NPY*) genes, which are involved in the appetite control.

In addition to cognitive symptoms, AD is also associated with noncognitive symptoms, which include alterations in hypothalamus-mediated feeding behaviors and body weight; these changes often precede cognitive impairments (Hiller and Ishii, 2018; Ishii and Iadecola, 2015). Notably, 3×Tg AD mice are less sensitive to cholecystokinin, a satiety factor, and have a decrease in the neuronal activity that modulates feeding behaviors (Adebakin et al., 2012). The noncognitive AD symptoms resulting from hypothalamic dysfunction are observed in patients with AD (Hiller and Ishii, 2018) and experimental AD transgenic mouse models (Do et al., 2018); however, the mechanism mediating hypothalamic dysfunction in AD is unclear.

Our previous studies have suggested that reciprocal augmentation between high-fat diet (HFD)-induced metabolic stress and AD central pathogenesis accelerates cognitive impairment and fatty liver disease in HFD-fed APP/PS1d9E (APP/PS1) transgenic mice (Lee et al., 2018; Shie et al., 2015; Yeh et al., 2015). Like HFD, the use of sugars and high-fructose corn syrup in the modern western diet contributes to the epidemic of obesity and metabolic disorders (Bray et al., 2004; Hannou et al., 2018; Malik et al., 2010; Mortera et al., 2019). High-sucrose diets (HSDs) have been shown to induce hyperglycemia, hyperinsulinemia, and fatty liver disease without increasing food intake and body mass in wild-type (WT) mice (Flister et al., 2018; Oliveira et al., 2014) and rats (Seshadri et al., 2019). Administration of sucrose-sweetened water induces a prediabetes stage in WT mice that includes glucose intolerance and hyperglycemia, which are followed by compensation via hyperinsulinemia and insulin resistance but without the development of obesity (Burgeiro et al., 2017). Intake of sucrose-sweetened water induces peripheral insulin resistance, accelerates memory deficits, and promotes amyloidosis in APP/PS1 mice (Cao et al., 2007; Orr et al., 2014). To date, no study has evaluated the impact of HSD on AD pathology. To compare the effects of HSD with those of normal chow diet (NCD), we used HSD pellet instead of sucrose-sweetened water.

This study evaluated whether HSD affects AD-related pathology and hypothalamic functionality. The body weight, glycemic regulation, neuroinflammation, and hypothalamic leptin signaling of HSD-fed WT and APP/PS1 mice were compared. The cognitive and noncognitive behaviors of WT and APP/PS1 mice fed either a NCD or HSD were investigated. Our findings reveal the deleterious effects of HSD on AD pathogenesis and provide novel insights into the role of leptin resistance on the noncognitive symptoms of AD.

2. Materials and methods

2.1. Animals

All animal handling procedures were approved by the Yang-Ming University Institutional Animal Care and Use Committee (IACUC No: 1041251, 30 December, 2015). APP/PS1 transgenic mice (B6.Cg-Tg[APPswe, PSEN1dE9]85Dbo/Mmjax; No. 005864) expressing a chimeric mouse/human APP695 that harbored Swedish K595N/M596L mutations (APPswe) and human PS1 with the exon-9 deletion mutation (PS1dE9) were purchased from the Mutant Mouse Resource and Research Center at the Jackson Laboratories and bred in-house. Mice were provided with food and water *ad libitum* and were housed under controlled room temperature (22 ± 2 °C) and humidity (55%–65%) under a 12:12 hours of light-dark cycle. The dark cycle lasted from 19:00 to 7:00. Nonalcoholic fatty liver disease (NAFLD) is a sexually dimorphic disease (Ballestri et al., 2017; Pape et al., 2018). Previously we found that HFD-induced NAFLD in APP/PS1 mice does not occur in female mice (Shie et al., 2015). The purpose of our present study was to create an animal model of NAFLD-like metabolic stress using HSD. Therefore, only male mice were used. More than 3 cohorts of male APP/PS1 mice and their WT littermates were randomly assigned to the various dietary manipulation groups at 10 weeks. One group was fed NCD containing carbohydrates at 50.0%, fat at 5.0%, and sucrose at 1.16% by weight (5010, Lab Diet, USA). These mice were designated as NCD WT and NCD APP/PS1 groups, respectively. The other groups were fed HSD containing carbohydrate at 67.3%, fat at 4.3%, and sucrose at 35% by weight (D12450B, Research Diet, USA), respectively. These mice were designated as HSD WT and HSD APP/PS1 groups. Fat content was comparable in the NCD and the HSD, and the major difference between the NCD and the HSD was the sucrose content.

2.2. Measurements of serum biochemical parameters

Blood samples were collected from the tail vein of male NCD WT, NCD APP/PS1, HSD WT, and HSD APP/PS1 mice to measure levels of leptin and soluble leptin receptors (LepRs) after a 16-hours (18:00 to 10:00) fasting at 6, 12, 20, and 28 weeks of dietary manipulation (Lee et al., 2018). A 4 hours (10:00–14:00), refeeding was performed after 16-hours fasting (18:00 to 10:00) after 20 weeks of dietary manipulation. The levels of leptin and LepRs were measured using enzyme-linked immunosorbent assay (ELISA) kits (R&D Systems, Minneapolis, MN, USA). The fluorescence intensity was measured at 450 nm.

2.3. Measurement of cortical and serum Aβ and IL-6

The levels of cortical Aβ40 and Aβ42 after 28 weeks of dietary manipulations were measured as previously described (Lee et al., 2018). The cerebral cortex was homogenized into phosphate buffer saline (PBS) containing 0.5% SDS, 0.5% Triton X-100, and 1 mM phenylmethylsulfonyl fluoride with protease inhibitor cocktail tablets (Roche Diagnostics, Indianapolis, IN, USA). After sonication and centrifugation, the supernatant was designated as the SDS-soluble fraction. The pellet was suspended in 3 M guanidine-HCl and sonicated. After centrifugation, the supernatant was designated as the SDS-insoluble fraction. The levels of Aβ40 and Aβ42 in the cerebral cortex and serum were measured using Aβ ELISA kits (Invitrogen, CA). The serum levels of interleukin 6 (IL-6) were measured by ELISA according to the manufacturer's instructions (R&D Systems, Minnesota, MN, USA) at a sensitivity of 7 pg/mL.

2.4. Leptin-induced feeding suppression

Singly housed mice from each group were acclimated with a food container (Oriental Yeast Co, Ltd, Japan) for one week. The daily food intake was recorded using a food container over the first 3 days after the dietary switch and after 23 weeks of dietary manipulation. Leptin-induced feeding suppression of HSD WT and APP/PS1 mice after 28 weeks of dietary manipulation was performed as previously described with minor modifications (Tillman et al., 2014). Briefly, mice were injected intraperitoneally with mouse recombinant leptin (R&D Systems, Minneapolis, MN, USA) at a dose of either 4 mg/kg leptin or PBS at 18:30. Food pellets in a food

container were provided at the beginning of the dark cycle (19:00) and after 4, 8, and 12 hours the cumulated food intake was measured.

2.5. Assessment of locomotor activity and daily living capability

Assessment consisting of the open field test, nesting, burrowing, and marble burying were performed after 26–27 weeks of dietary manipulation. The open field test was performed as described previously (Yeh et al., 2015). Mice were placed in a plastic box (40 cm × 40 cm × 38 cm) and allowed to explore freely for 30 minutes (19:00 to 19:30). Data were analyzed by EthoVision video tracking system (Noldus Information Technology, Netherlands). To record nesting behavior, mice were housed individually with 2 pieces of Nestlet (Ancare, UK agent, Lillico) as described previously (Yeh et al., 2015). After 16 hours, the constructed nest was scored from 1 to 5 according to Deacon's system (Deacon, 2006) and the unshredded Nestlet was weighed. The time to complete the nest (rating score 5) was recorded. Marble burying was performed as described previously (Thomas et al., 2009). Mice were allowed to freely explore a cage containing marbles for 30 minutes and then the number of marbles buried was counted. The burrowing test was performed as described previously (Tzeng et al., 2018). Mice were housed individually and allowed to habituate for 24 hours. The burrowing devices were filled with 230 g food pellets and placed into cages. The amount of food pellets left in the burrows was recorded after 2 hours.

2.6. Food entrainment test

The food entrainment test was performed as described previously with some modifications (Mieda et al., 2006). A schematic diagram of the food entrainment test is shown in Fig. 5A. Briefly, male APP/PS1 and WT mice that had been fed either NCD or HSD were singly housed at 24 weeks after dietary manipulation. Two NCD or HSD food pellets were placed on the cage floor and replaced with fresh food every day at 11:00 for 3 days; this was designated as *ad libitum* feeding (ALF) period. The home-cage mobility of mice was recorded for 24 hours on day 3 of ALF period. The next day, 2 food pellets were put on cage floor at 11:00 and then the leftover food was removed at 15:00 for 9 days; this was designated the restricted feeding (RF) period. The home-cage mobility was recorded for 24 hours on the day 9 of RF. On day 10, the mice were given no food; this was designated the no food (NF) period. The mobility of mice on the day of NF was also recorded for 24 hours.

2.7. Immunohistochemical and histochemical staining

After 28 weeks of dietary manipulation, mice from the various groups were perfused with 4% paraformaldehyde, and their brain tissues were cryoprotected. Free-floating brain sections (Bregma: −1.72 to −2.20) were incubated with mouse anti-pSTAT3 (1:1000, Sigma) overnight at 4 °C. After washes, the brain sections were incubated with biotinylated secondary antibodies (1:1000, Sigma) for 2 hours at room temperature. The sections were then washed with 1× Tris-buffered saline and incubated with ABC reagent. Next, the DAB coloring reaction was performed. Areas identified as the ARC, VMH, and DMH were defined by the presence of clustered nuclei stained with DAPI or Neutral Red before pSTAT3 immunohistochemical staining. The numbers of pSTAT3-positive cells were quantified using ImageJ software (the National Institutes of Health, USA) after converting the color images to grayscale. The cells with pSTAT3 intensity above the 0–100 threshold setting in ImageJ software were counted as pSTAT3-positive cells as described previously (Lee et al., 2018). Finally, a visual inspection of each brain slice was carried out to confirm that the cells counted by ImageJ were pSTAT3 positive. The numbers of pSTAT3-positive cells present in 2 to 3 sequential slices were averaged. To detect double staining of senile plaques and astrocytes, brain sections were stained with Amylo-Glo RTD amyloid staining reagent (1:100, Biosensis) and then were washed in PBS with Tween-20. Next, the brain slices were incubated with mouse anti–glial fibrillary acidic protein (GFAP) antibody (1:5000, Sigma) at 4 °C overnight. After washes, the brain slices were incubated with donkey anti-mouse Alexa Fluor 594 secondary antibody (1:500, Alexa). After washes, the sections were mounted in Aqua Poly/Mount (Polyscience Inc, Warrington, PA, USA) and images were captured using Zeiss Axioplan 2 microscope. The coverage of senile plaques and GFAP fluorescent intensity were quantified using ImageJ.

2.8. RNA extraction and real-time PCR

After 28 weeks of dietary manipulation, the cortex of one hemisphere from mice of the 4 groups and the whole hypothalamus from mice of HFD groups were homogenized in TRIzol reagent and total RNA was prepared (Invitrogen, Camarillo, CA, USA), RNA (2–5 μg). Each RNA sample was reverse-transcribed into cDNA using SuperScript III reverse transcriptase (Invitrogen, Camarillo, CA, USA). Real-time PCR was then performed using the StepOnePlus Real-Time PCR System using 5 μL cDNA, SYBR Green (Invitrogen, Camarillo, CA, USA), 10 mM primer, and 10 mM dNTP. The cycling conditions were 10 minutes at 95 °C, followed by 40 cycles of 15 seconds at 95 °C, and then 60 seconds at 60 °C. Threshold cycle (Ct) values for each test gene were normalized against the Ct values of actin control. The ratio of each gene was calculated as $2^{-(\Delta\Delta Ct)}$, in which ΔΔCt represents [(Ct gene of interest–Ct internal control) sample A–(Ct gene of interest–Ct internal control) sample B]. The primer pairs used are presented in Table 1.

2.9. Accurately aligned whole-body anatomical microcomputed tomography for fat mass comparison

Mice were anesthetized using isoflurane after 6, 10, and 20 weeks of dietary manipulation. Images were acquired using microcomputed tomography (MILabs, Utrecht, Netherlands). The range of images in length was 79.5 mm, and mice were imaged using 480 projections. The X-ray parameters were set at 0.48 mA and 50 kV. Finally, an image voxel was constructed using 80 μm. The images were analyzed using PMOD 3.8 (PMOD Technologies LTD, Zurich, Switzerland). The image matrix was reduced by 2 × 2 × 2 at first and segmented into different body compositions according to tissue density. The threshold for fat tissue was −400 ~ −200 HU. After acquiring the volumes in voxels in cm^3 for fat tissue, the

Table 1
Primer sets used to investigate the expression levels of genes involved in inflammation and energy homeostasis

	Forward primer	Reverse primer
IL-6	GCCTTCCCTACTTCACAAGT	GAATTGCCATTGCACAACTCT
IL-1β	TTGAAGAAGAGCCCATCCTC	CAGCTCATATGGGTCCGAC
GFAP	CGAGTCCCTAGAGCGGCAAATG	CGGATCTGGAGGTTGGAGAAAGTC
Iba-1	GGATTTGCAGGGAGGAAAAG	TGGGATCATCGAGGAATTG
NPY	CTCCGCTCTGCGACACTAC	AATCAGTGTCTCAGGGCT
AgRP	ATGCTGACTGCAATGTTGCTG	CAGACTTAGACCTGGGAACTCT
POMC	ATGCCGAGATTCTGCTACAG	TGCTGCTGTTCCTGGGGC
SOSC3	GCGGGCACCTTTCTTATCC	TCCCCGACTGGGTCTTGAC
Actin	CATTGCTGACAGGATGCAGAAGG	TGCTGGAAGGTGGACAGTGAGG

Table 2
Two-way ANOVA of the interactions between dietary manipulation and genotypes for biochemical indices

	Interaction $F_{interaction\ (df)}$ *p* value	Main effect $F_{group\ (df)}$ *P* value		Simple main effect $F_{group\ (df)}$ *p* value			
		Diet	Genotype	NCD	HSD	WT	APP/PS1
Cortex inflammatory mRNA level (DM 28 w)							
GFAP	$F_{(1,17)} = 19.429$ $p < 0.001$			$F_{(1,9)} = 0.373$ $p = 0.556$	$F_{(1,8)} = 31.837$ $p < 0.001$	$F_{(1,10)} = 3.023$ $p = 0.113$	$F_{(1,7)} = 27.469$ $p < 0.005$
IL-1β	$F_{(1,16)} = 14.715$ $p < 0.01$			$F_{(1,8)} = 0.227$ $p = 0.647$	$F_{(1,8)} = 59.976$ $p < 0.001$	$F_{(1,10)} = 1.418$ $p = 0.261$	$F_{(1,6)} = 11.686$ $p < 0.05$
Iba-1	$F_{(1,17)} = 1.873$ $p = 0.189$	$F_{(1,1)} = 0.259$ $p = 0.617$	$F_{(1,1)} = 9.141$ $p < 0.01$				
Hypothalamic downstream genes of leptin signaling (DM 28 w)							
POMC	$F_{(1,17)} = 12.644$ $p < 0.005$			$F_{(1,6)} = 18.871$ $p < 0.01$	$F_{(1,11)} = 7.562$ $p < 0.05$	$F_{(1,11)} = 8.707$ $p < 0.05$	$F_{(1,6)} = 14.216$ $p < 0.01$
AgRP	$F_{(1,16)} = 3.980$ $p = 0.063$	$F_{(1,1)} = 8.898$ $p < 0.01$	$F_{(1,1)} = 0.761$ $p = 0.396$				
SOCS3	$F_{(1,16)} = 0.147$ $p = 0.707$	$F_{(1,1)} = 7.134$ $p < 0.05$	$F_{(1,1)} = 0.390$ $p = 0.541$				
Iba-1	$F_{(1,16)} = 1.873$ $p = 0.986$	$F_{(1,1)} = 0.151$ $p = 0.703$	$F_{(1,1)} = 4.575$ $p < 0.05$				
Blood glucose, insulin and HOMA-IR (DM 12 w)							
Blood glucose	$F_{(1,16)} = 0.006$ $p = 0.938$	$F_{(1,1)}$=225.92 $p < 0.001$	$F_{(1,1)} = 3.561$ $p = 0.077$				
Insulin	$F_{(1,16)}$ =1.360 $p = 0.261$	$F_{(1,1)} = 26.00$ $p < 0.001$	$F_{(1,1)} = 19.227$ $p < 0.001$				
HOMA-IR	$F_{(1,16)} = 2.660$ $p = 0.122$	$F_{(1,1)} = 54.52$ $p < 0.001$	$F_{(1,1)} = 16.183$ $p < 0.005$				
Body weight							
(DM 24 w)	$F_{(1,53)} = 0.598$ $p = 0.443$	$F_{(1,1)} = 27.05$ $p < 0.001$	$F_{(1,1)} = 0.71$ $p = 0.403$				
(DM 28 w)	$F_{(1,57)}$ =0.032 $p = 0.859$	$F_{(1,1)} = 21.37$ $p < 0.001$	$F_{(1,1)} = 5.43$ $p < 0.05$				
Fat content (DM 20 w)	$F_{(1,35)} = 0.022$ $p = 0.884$	$F_{(1,1)} = 19.88$ $p < 0.001$	$F_{(1,1)} = 1.044$ $p = 0.314$				
Leptin							
Refeeding (DM 20 w)	$F_{(1,21)} = 0.039$ $p = 0.845$	$F_{(1,1)} = 19.80$ $p < 0.001$	$F_{(1,1)} = 0.342$ $p = 0.565$				
Soluble leptin receptor							
Non-fasting (DM 20 W)	$F_{(1,24)} = 7.520$ $p < 0.05$			$F_{(1,12)} = 0.518$ $p = 0.485$	$F_{(1,12)} = 6.774$ $p < 0.05$	$F_{(1,14)}$= 115.473 $p < 0.001$	$F_{(1,10)}$ =40.959 $p < 0.001$
Fasting (DM 20 W)	$F_{(1,30)} = 4.273$ $p < 0.05$			$F_{(1,14)} = 0.005$ $p = 0.944$	$F_{(1,16)} = 6.079$ $p < 0.05$	$F_{(1,16)} = 50.519$ $p < 0.001$	$F_{(1,14)} = 8.790$ $p < 0.05$
Refeeding (DM 20 W)	$F_{(1,21)} = 0.509$ $p = 0.483$	$F_{(1,1)} = 29.95$ $p < 0.001$	$F_{(1,1)} = 0.684$ $p = 0.418$				
Fasting (DM 28 W)	$F_{(1,28)} = 3.544$ $p = 0.070$	$F_{(1,1)} = 60.32$ $p < 0.001$	$F_{(1,1)} = 0.053$ $p = 0.820$				

Key: AgRP, Agouti-related protein; ANOVA, analysis of variance; APP/PS1, APP/PS1 genetic background; (df), degree of freedom; DM, diet manipulation; DM, weeks after the diet manipulations; GFAP, glial fibrillary acidic protein; HSD, high-sucrose diet; HOMA-IR, homeostasis model assessment for insulin resistance index; Iba-1, ionized calcium-binding APP/PS1 adaptor molecule 1; IL-1β, interleukin-1 β; LepRs, soluble leptin receptor; NCD, normal chow diet; NPY, neuropeptide Y; POMC, pro-opiomelanocortin; SOSC3, suppressor of cytokine signaling; WT, wild type.

amount of body fat was presented in grams and then the percentage of fat mass of the 4 groups was calculated.

2.10. Statistical analysis

Statistics were performed using GraphPad Prism 6 (GraphPad, CA, USA). All values are given as means ± standard error of the mean. All experiments were performed more than 3 times. Comparisons between 2 groups were carried out using an unpaired Student's *t*-test. To compare multiparametric analysis, one-way analysis of variance (ANOVA) followed by Bonferroni post hoc analysis. Two-way ANOVA (general linear model) was used to analyze the interaction between dietary manipulation and genotype for the biochemical indices, leptin-induced pSTAT3 upregulation, and the multiple behavioral tests; the results are shown in Tables 2–4. Nonparametric statistical tests (the Kruskal-Wallis test followed by Dunn's multiple comparison test) were used for the score of nesting. A *p* value less than 0.05 was considered to show a significant difference.

3. Results

3.1. The level of neuroinflammation of high-sucrose diet–fed APP/PS1 mice is elevated

The impact of a HSD on AD pathogenesis was assessed by comparing the senile plaque burden and glial activation between NCD-fed WT and APP/PS1 mice (designated as NCD WT and NCD APP/PS1 groups) and HSD-fed WT and APP/PS1 mice (designated as HSD WT and HSD APP/PS1 groups) after 28 weeks of dietary manipulation. Amylo-Glo RTD amyloid staining reagent was used to detect senile plaques; anti-GFAP antibody was used to detect reactive astrocytes. The fluorescent images showed that activated astrocytes clustered at the foci of the senile plaques in the cortices of NCD and HSD APP/PS1 mice (Fig. 1A). The expression of GFAP was low, and senile plaques were not detected in the cortices of NCD and HSD WT mice. The coverage of senile plaques in NCD and HSD APP/PS1 mice was not different (data not shown). The ratio of GFAP coverage and senile plaque coverage of HSD APP/PS1 mice

Table 3
Two-way ANOVA of the interactions between treatments and genotypes for the number of pSTAT3-positive cells in the hypothalamic nuclei

	Interaction $F_{interaction\ (df)}$ p value	Main effect $F_{group\ (df)}$ p value		Simple main effect $F_{group\ (df)}$ p value			
		Treatment	Genotype	PBS	Leptin	WT	APP/PS1
Number of pSTAT3-positive cells (DM 28 w)							
ARC	$F_{(1,17)} = 1.090$ $p = 0.311$	$F_{(1,1)} = 66.160$ $p < 0.001$	$F_{(1,1)} = 0.062$ $p = 0.807$				
VMH	$F_{(1,17)} = 29.099$ $p < 0.001$			$F_{(1,10)} = 0.157$ $p = 0.700$	$F_{(1,7)} = 26.43$ $p < 0.005$	$F_{(1,9)} = 97.13$ $p < 0.001$	$F_{(1,8)} = 138.18$ $p < 0.001$
DMH	$F_{(1,17)} = 16.234$ $p < 0.005$			$F_{(1,10)} = 0.374$ $p = 0.554$	$F_{(1,7)} = 16.2p < 0.01$	$F_{(1,9)} = 74.34$ $p < 0.001$	$F_{(1,8)} = 54.98$ $p < 0.001$

Key: APP/PS1, APP/PS1 genetic background; ANOVA, analysis of variance; ARC, arcuate nucleus; DMH, dorsomedial hypothalamus; (df), degree of freedom; DM, diet manipulations; PBS, phosphate buffer saline; VMH, ventromedial hypothalamus; WT, wild type.

was marginally, but not significantly, higher than that of NCD APP/PS1 mice ($F_{(1,\ 9)} = 4.984$, $p = 0.108$) (Fig. 1B). The ratio of GFAP intensity and senile plaque coverage of HSD APP/PS1 mice was not significantly higher than that of NCD APP/PS1 mice ($F_{(1,\ 9)}$=3.357, $p = 0.199$) (Fig. 1C). The ratio of GFAP coverage and GFAP intensity versus senile plaque coverage shows a trend toward elevation in HSD APP/PS1 mice, and therefore, the expression levels of *GFAP* and inflammatory cytokines were compared by RT-PCR (Fig. 1D–G). The cortical mRNA levels of *GFAP* and interleukin 1β (IL-1β) genes of HSD APP/PS1 mice were higher than those of NCD APP/PS1 and HSD WT mice (Fig. 1D and E). The cortical mRNA level of ionized calcium-binding adaptor molecule 1 in HSD APP/PS1 mice was higher than in HSD WT mice (Fig. 1F). However, the cortical mRNA level of IL-6 did not differ across the 4 groups (Fig. 1G).

Next, ELISA was performed to quantify the levels of Aβ of 4 groups after 28 weeks of dietary manipulation. The cortical levels of SDS-soluble and SDS-insoluble Aβ40 and Aβ42 were significantly increased in HSD APP/PS1 mice compared with NCD APP/PS1 mice (Fig. 1H and I). As expected, Aβ40 and Aβ42 were not detected in NCD WT and HSD WT mice. Soluble Aβ present in peripheral circulation has been shown to induce systematic glucose dysregulation and insulin insensitivity of the liver (Bomfim et al., 2012; Zhang et al., 2013), and then we next examined the serum levels of Aβ and IL-6 after 28 weeks of dietary manipulation. Serum Aβ was significantly elevated in HSD APP/PS1 mice compared with NCD APP/PS1 mice (Fig. 1J).

Serum IL-6 was undetectable in NCD WT mice (Fig. 1K). Furthermore, the level of serum IL-6 present in HSD APP/PS1 mice was higher than that of HSD WT mice. These findings suggest that both peripheral inflammation status and central neuroinflammation were exacerbated in HSD APP/PS1 mice. In addition, pSTAT3-positive cells were detected in the cortices of APP/PS1 mice (Supplemental Fig. 1), and this has been shown to be mediated by IL-6 (Kim et al., 2016). No pSTAT3-positive cells were detected in the cortices of WT groups. The pSTAT3-positive cells were also present in the hippocampus of APP/PS1 mice but not in the hippocampus of WT groups (data not shown). Our data indicated that HSD and AD pathology augments inflammation and Aβ levels in the CNS and periphery. Two-way ANOVA indicated that HSD interacts with APP/PS1 genetic background on the upregulation of GFAP and IL-1β mRNA in the mouse cortex (Table 2).

3.2. A high-sucrose diet increases fat mass before increasing body weight

Previous studies have shown that insulin resistance can be induced by HSD in WT rodents (Apolzan and Harris, 2013; Oliveira et al., 2014; Schultz et al., 2015) and by sucrose-sweetened water in

Table 4
Two-way ANOVA of the interactions between dietary manipulation and genotypes for food-entrainable behavior, marble burying, nesting, and burrowing

	Interaction $F_{interaction\ (df)}$ p value	Main effect $F_{group\ (df)}$ p value		Simple main effect $F_{group\ (df)}$ p value			
		Diet	Genotype	NCD	HSD	WT	APP/PS1
Food-entrainable behavior (DM 23 w)							
RF distance	$F_{(1,43)} = 0.040$ $p = 0.842$	$F_{(1,1)} = 37.022$ $p < 0.001$	$F_{(1,1)} = 0.665$ $p = 0.419$				
NF distance	$F_{(1,43)} = 8.057$ $p < 0.01$			$F_{(1,25)} = 0.359$ $p = 0.555$	$F_{(1,18)} = 45.99$ $p < 0.001$	$F_{(1,22)} = 0.003$ $p = 0.956$	$F_{(1,21)} = 17.357$ $p < 0.001$
Marble burying (DM 26–27 w)	$F_{(1,56)}$ =3.078 $p = 0.085$	$F_{(1,1)} = 7.063$ $p < 0.05$	F(1,1) =4.748 $p < 0.05$				
Nesting (DM 26–27 w)							
Nest score			$F_{(1,38)} = 1.918$ $p = 0.174$	$F_{(1,1)} = 7.198$ $p < 0.05$			
Unshredded Nestlet	$F_{(1,38)} = 0.709$ $p = 0.405$	$F_{(1,1)} = 12.616$ $p < 0.005$	$F_{(1,1)} = 10.622$ $p < 0.005$				
Nest completed time	$F_{(1,38)} = 0.857$ $p = 0.360$	$F_{(1,1)} = 6.565$ $p < 0.05$	$F_{(1,1)} = 25.921$ $p < 0.001$				
Burrowing (DM 26–27 w)	$F_{(1,54)} = 2.395$ $p = 0.128$	$F_{(1,1)} = 6.494$ $p < 0.05$	$F_{(1,1)} = 2.607$ $p = 0.112$				

Key: APP/PS1, APP/PS1 genetic background; ANOVA, analysis of variance; (df), degree of freedom; DM, diet manipulations; HSD, high-sucrose diet; NCD, normal chow diet; NF, no food during the expected feeding period; RF, restricted feeding; WT, wild type.

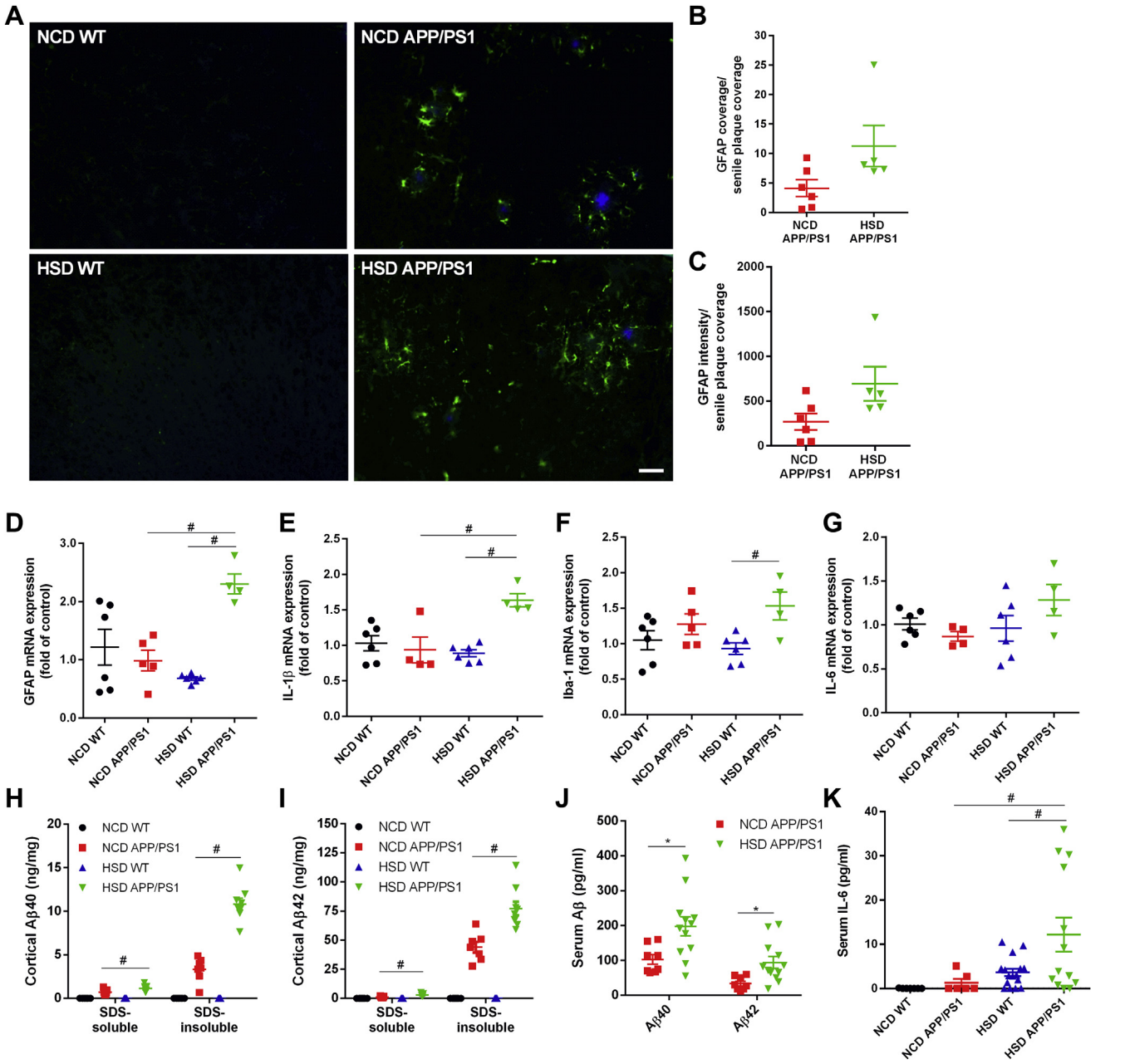

Fig. 1. HSD elevates neuroinflammation and peripheral inflammation in APP/PS1 mice. (A) Representative fluorescent images of senile plaques (blue) and GFAP (green) in the cortex of NCD WT ($n = 6$), NCD APP/PS1 ($n = 5$), HSD WT ($n = 6$), and HSD APP/PS1 ($n = 5$) mice. Scale bar, 20 μm. (B) The ratio of GFAP coverage to senile plaque coverage of HSD WT ($n = 6$) and HSD APP/PS1 ($n = 5$) mice. (C) The ratio of GFAP intensity to senile plaque coverage of HSD WT ($n = 6$) and HSD APP/PS1 ($n = 5$) mice. (D–G) Quantification of mRNA expression levels of *GFAP* (D), *IL-1β* (E), *Iba-1* (F), and *IL-6* (G) genes in the cortex of NCD WT mice ($n = 6$), NCD APP/PS1 mice ($n = 5$), HSD WT mice ($n = 6$), and HSD APP/PS1 mice ($n = 4$). (H and I) The cortical levels of Aβ40 (H) and Aβ42 (I) of NCD WT mice ($n = 8$), NCD APP/PS1 mice ($n = 7$), HSD WT mice ($n = 9$), and HSD APP/PS1 mice ($n = 9$) were measured. (J) The serum levels of Aβ40 and Aβ42 of NCD APP/PS1 mice ($n = 8$) and HSD APP/PS1 mice ($n = 12$) were measured. (K) The serum levels of IL-6 of NCD WT mice ($n = 6$), NCD APP/PS1 mice ($n = 6$), HSD WT ($n = 16$), and APP/PS1 mice ($n = 13$) were measured. Data are expressed as mean ± SEM. Statistical differences between groups were determined by one-way ANOVA followed by Bonferroni *post hoc* tests and are labeled using # ($p < 0.05$). Statistical differences between groups were determined by unpaired Student's *t*-test and are labeled with *($p < 0.05$) (B, C, and J). Abbreviations: ANOVA, analysis of variance; GFAP, glial fibrillary acidic protein; HSD, high-sucrose diet; NCD, normal chow diet; WT, wild type. (For interpretation of the references to color in this figure legend, the reader is referred to the Web version of this article.)

3×Tg AD mice (Orr et al., 2014). Whether or not glucose homeostasis in APP/PS1 mice is altered by HSD was assessed in this study. The glucose levels between 4 groups were not different after 6–7 weeks of dietary manipulation (Supplemental Fig. 2). However, after 12 weeks of dietary manipulation, the glucose levels of HSD groups were significantly higher than that of NCD groups. The insulin levels of HSD APP/PS1 mice were elevated, whereas the glucose levels of HSD WT and HSD APP/PS1 mice were comparable (Fig. 2A and B). The homeostasis model assessment for insulin resistance index results, which acts as an indirect measure of insulin resistance, suggested that insulin resistance was higher in HSD APP/PS1 mice (Fig. 2C).

The body weight between the 4 groups was not different after 20 weeks of dietary manipulation. Over that time, however, there was a trend toward weight gain in HSD groups. The body weights of HSD groups were significantly higher than that of NCD groups after 24 weeks of dietary manipulation (Fig. 2D). However, the body weights were not different between HSD APP/PS1 and WT mice.

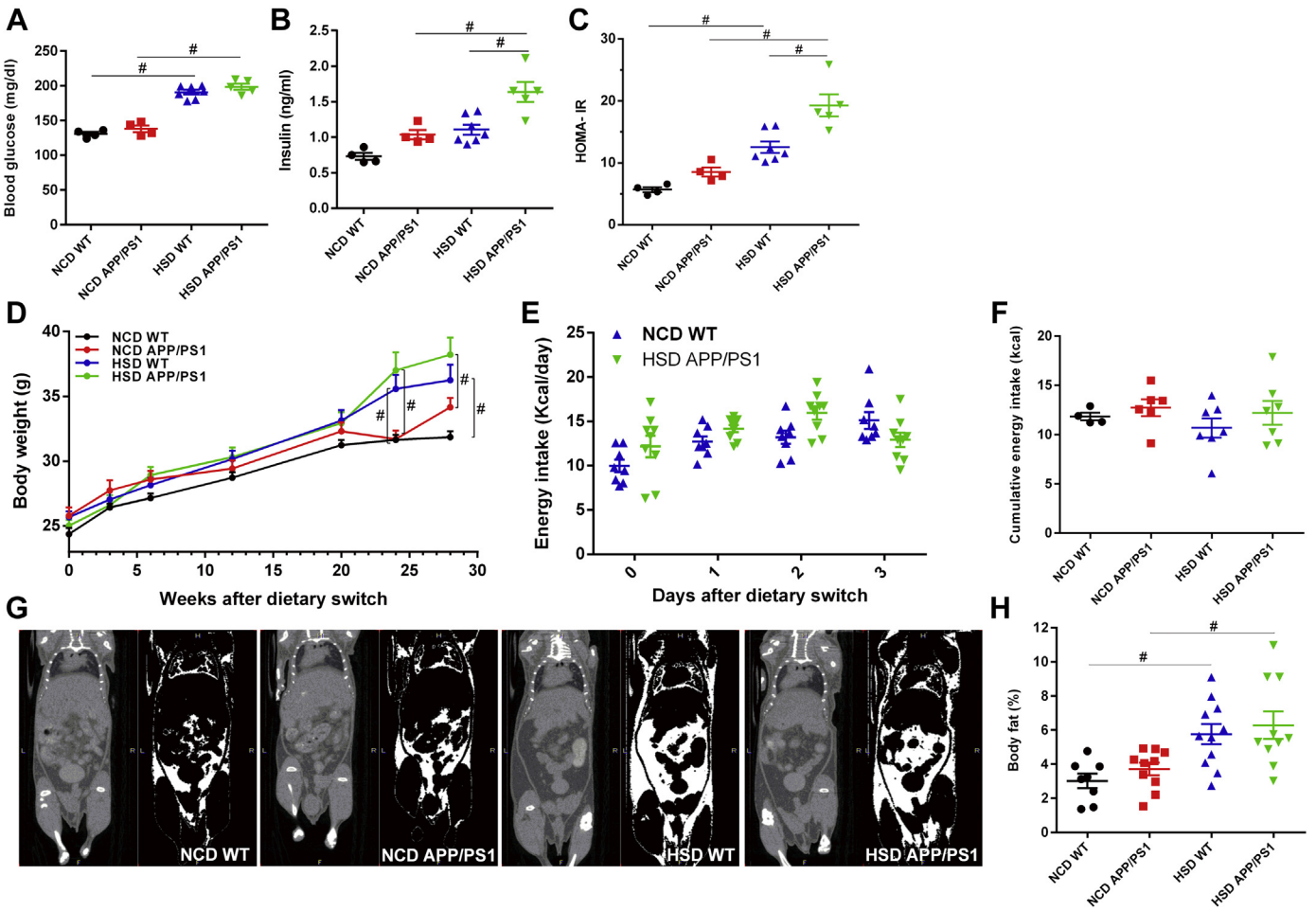

Fig. 2. Insulin resistance is exacerbated in HSD APP/PS1 mice with comparable body weight gain and fat mass relative to HSD WT mice. The levels of fasting glucose (A) and insulin (B) of NCD WT ($n = 4$), NCD APP/PS1 ($n = 4$), HSD WT ($n = 7$), and HSD APP/PS1 mice ($n = 5$) after 12 wk of dietary manipulation. (C) HOMA-IR calculation. (D) Body weight curves for NCD WT mice ($n = 8$), NCD APP/PS1 mice ($n = 10$), HSD WT mice ($n = 11$), and HSD APP/PS1 mice ($n = 10$). (E) Energy intake of WT mice (n = 8) and APP/PS1 mice (n = 9) for the first 3 d after the dietary switch from NCD to HSD. (F) The daily energy intakes of NCD WT mice ($n = 4$), NCD APP/PS1 mice ($n = 6$), HSD WT mice ($n = 7$), and HSD APP/PS1 mice ($n = 7$) were measured after 23 wk of dietary manipulation. (G) Representative images taken by microcomputed tomography of the 4 groups after 20 wk of dietary manipulation. (H) The percentages of fat mass present in NCD WT mice ($n = 8$), NCD APP/PS1 mice ($n = 10$), HSD WT mice ($n = 11$), and HSD APP/PS1 mice ($n = 10$) were calculated. Data are expressed as mean ± SEM. Significant differences between groups were determined by one-way ANOVA followed by Bonferroni *post hoc* tests and are labeled using # ($p < 0.05$). Abbreviations: ANOVA, analysis of variance; HSD, high-sucrose diet; NCD, normal chow diet; WT, wild type.

Whether excess food intake was induced by HSD was examined. HSD did not induce a higher daily energy intake in the first 3 days after the dietary switch (Fig. 2E). The daily energy intake of the 4 groups was not different after 23 weeks of dietary manipulation, although a trend toward weight gain in HSD groups compared with NCD groups could be observed between 20 to 24 weeks (Fig. 2F). These data indicate that the weight gain in HSD groups was not caused by hyperphagia. Our findings suggest that glycemic dysregulation is an earlier biomarker than body weight gain induced by HSD in APP/PS1 mice.

To determine whether the APP/PS1 genetic background or HSD alters lipogenesis, the body fat mass of the 4 groups was measured by microcomputed tomography. No difference was found in the fat mass of the 4 groups after 6 and 10 weeks of dietary manipulations (data not shown). Nevertheless, the fat mass of HSD groups, especially the visceral fat, was significantly greater than that of NCD groups after 20 weeks of dietary manipulation, as shown by the microcomputed tomography (Fig. 2G). One-way ANOVA suggested that HSD significantly increases fat mass compared with NCD in both WT and APP/PS1 mice before body weight differences between NCD and HSD groups (Fig. 2H). Two-way ANOVA indicated that both HSD and APP/PS1 genetic background had main effects on insulin levels, homeostasis model assessment for insulin resistance index, and body weight. Only HSD had a main effect on fat mass.

3.3. *Leptin resistance of HSD groups is induced in the absence of hyperleptinemia*

The body weight and fat mass of HSD groups are higher than those of NCD groups, and therefore, whether HSD induces hyperleptinemia was then assessed. Although the fat mass of HSD groups was higher than that of NCD groups, the fasting levels of leptin were not different among the 4 groups, and after dietary manipulation for 6 weeks: $F_{(1, 32)} = 3.149$, $p = 0.0684$, after dietary manipulation for 12 weeks: $F_{(1, 32)} = 2.557$, $p = 0.0725$; and after dietary manipulation for 28 weeks: $F_{(1, 32)} = 0.157$, $p = 0.6764$ (Fig. 3A).

LepRs released by the liver are able to bind to leptin and reduce the level of effective leptin in the bloodstream (Schulz and Widmaier, 2006). Therefore, we investigated whether HSD regulates the serum levels of LepRs. The level of fasting LepRs of HSD WT mice was higher than that of NCD WT mice after 6, 12, and 28 weeks of dietary manipulation (Fig. 3B). The level of fasting LepRs of HSD APP/PS1 mice was higher than that of NCD APP/PS1 mice only after

28 weeks of dietary manipulation. These findings suggest that a higher level of free leptin was available for transport into the CNS of HSD APP/PS1 mice compared with HSD WT mice after 6 and 12 weeks of dietary manipulation.

Fasting acts as a signal to the body that energy stores need to be replenished. The serum level of leptin and LepRs in response to refeeding after a 16-hours fast was examined after 20 weeks of dietary manipulation to assess the response of adipose tissue and the liver to an altered energy status when the body weight of 4 groups was not different (Knights et al., 2014). The level of leptin of the 4 groups was decreased in response to a 16-hours fast (Fig. 3C). The leptin levels of NCD groups after refeeding were similar to nonfasting levels, suggesting that the release of leptin by white adipose tissues of NCD groups was similar during refeeding and nonfasting. However, the leptin level of HSD groups was significantly higher than that of NCD groups after refeeding. This result suggests that the white adipose tissue of HSD groups release greater amounts of leptin in response to energy replenishment.

The level of LepRs in HSD groups was higher than that of NCD groups during nonfasting, fasting, and refeeding. This result suggests that the livers of HSD groups released more LepRs that then bind to leptin in circulation compared with NCD groups (Fig. 3D). The level of LepRs in HSD WT mice was higher than in HSD APP/PS1 mice during nonfasting and fasting, but not during refeeding. Therefore, refeeding elevated the levels of leptin and LepRs in HSD WT and APP/PS1 mice equally. This suggests that the liver and adipose tissue of HSD APP/PS1 mice functioned as well as those of HSD WT mice during energy replenishment (Fig. 3C and D). Taken together with the increased body weight and the greater fat mass of HSD groups, the higher leptin levels induced by refeeding in HSD groups prompted us to examine whether leptin sensitivity was altered by HSD after 28 weeks of dietary manipulation. Leptin was intraperitoneally injected once into mice in each of the 4 groups and food intake was measured at 4, 8, and 12 hours after refeeding (Fig. 3E). The cumulative food intake of NCD groups was reduced by leptin. However, the food intake of HSD groups was not different with or without the leptin injection. These findings suggest that leptin sensitivity was reduced in HSD groups.

Two-way ANOVA showed that HSD interacted with APP/PS1 genetic background at the level of nonfasting LepRs and fasting LepRs (Table 2). Furthermore, HSD had a main effect on the levels of leptin and LepR after refeeding.

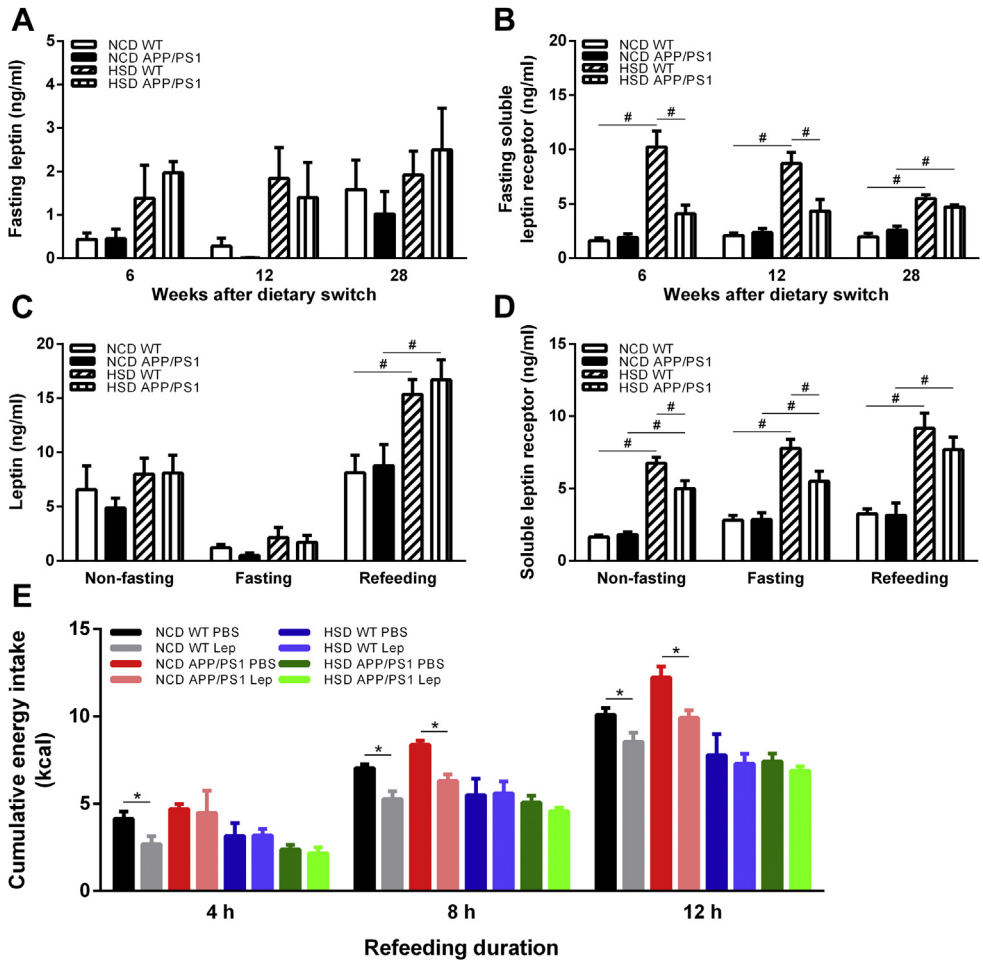

Fig. 3. HSD induces leptin resistance in the absence of hyperleptinemia. Levels of fasting leptin in NCD WT mice ($n = 9, 9, 9$), NCD APP/PS1 mice ($n = 9, 9, 8$), HSD WT mice ($n = 9, 9, 7$), and HSD APP/PS1 mice ($n = 9, 9, 6$) were measured at 6, 12, and 28 wk after dietary manipulation, respectively (A). Levels of LepRs in NCD WT mice ($n = 9, 9, 9$), NCD APP/PS1 mice ($n = 8, 9, 9$), HSD WT mice ($n = 9, 9, 8$), and HSD APP/PS1 mice ($n = 9, 8, 6$) were measured at 6, 12, and 28 wk after dietary manipulation, respectively (B). Levels of leptin (C) and LepRs (D) in NCD WT mice ($n = 7, 9, 6$), NCD APP/PS1 mice ($n = 7, 7, 5$), HSD WT mice ($n = 9, 9, 9$), and HSD APP/PS1 mice ($n = 5, 9, 5$) for the nonfasting, fasting, and refeeding after fasting states, respectively, were measured after 20 wk of dietary manipulations. (E) The cumulative energy intakes of NCD WT ($n = 7$), NCD APP/PS1 ($n = 7$), HSD WT ($n = 9$), and HSD APP/PS1 ($n = 9$) mice after an i.p. injection of leptin (Lep) or the vehicle were measured after 28 wk of dietary manipulation. Data are expressed as mean ± SEM. Significant differences between groups were determined by one-way ANOVA followed by Bonferroni *post hoc* tests and are labeled using # ($p < 0.05$). Comparisons between two groups were carried out using an unpaired Student's *t*-test. A p value less than 0.05 was considered to show a significant difference and labeled using *. Abbreviations: ANOVA, analysis of variance; HSD, high-sucrose diet; NCD, normal chow diet; WT, wild type.

3.4. Leptin signaling is attenuated at the VMH and DMH of HSD APP/PS1 mice

Senile plaques and GFAP upregulation in the hypothalamus of APP/PS1 mice was not detected by Amylo-Glo staining and GFAP immunohistochemistry staining, respectively, after 28 weeks of dietary manipulation (Supplemental Fig. 3A). However, leptin sensitivity is attenuated by HSD, and therefore, we examined whether leptin signaling in the hypothalamus is different for HSD WT and APP/PS1 mice by comparing the number of pSTAT3-positive cells in the mediobasal hypothalamus of HSD groups after injection with either leptin or vehicle (PBS) (Fig. 4A). Initially, the specificity of anti-pSTAT3 antibody was examined by using alkaline phosphatase to eliminate the immunohistochemical signal of pSTAT3 (Supplemental Fig. 4A). In addition, the nuclear compartmentalization of pSTAT3 after leptin injection was confirmed by confocal imaging in the hypothalamus (Supplemental Fig. 4B and C). Leptin-induced pSTAT3 in the hypothalamus of WT and APP/PS1 mice was quantified after 28 weeks on HSD. The level of leptin-induced pSTAT3 in the ARC was similar to that found in HSD APP/PS1 and WT mice (Fig. 4B). Nevertheless, the level of leptin-induced pSTAT3 in the VMH and DMH of HSD APP/PS1 mice was attenuated compared with that of HSD WT mice (Fig. 4C and D).

Next, we examined whether the mRNA levels of leptin downstream genes that mediate satiety were altered by HSD in the hypothalamus. The mRNA expression levels of *AgRP* and *POMC* genes were found to be upregulated by HSD in the hypothalamus of WT mice but not in the hypothalamus of APP/PS1 mice (Fig. 4E and F). Our results suggest that there is differential regulation of these leptin downstream genes between WT and APP/PS1 mice in the hypothalamus after 28 weeks on HSD. However, the mRNA expression levels of *NPY*, suppressor of cytokine signaling 3 (*SOCS3*), *GFAP*, and *Iba-1* were found not to be different when these 4 groups were compared (Supplemental Fig. 3B–E). Therefore, HSD attenuated leptin signaling in APP/PS1 mice, including a reduction of hypothalamic pSTAT3-positive cells and the leptin downstream target genes and that this occurs before the presence of senile plaques and astrocyte activation.

Two-way ANOVA showed that leptin treatment interacted with APP/PS1 genetic background with respect to the number of pSTAT3-positive cells in the VMH and DMH after 28 weeks on HSD (Table 3). HSD interacted with APP/PS1 genetic background on mRNA level of *POMC* gene in the hypothalamus. HSD had a main effect on mRNA levels of *AgRP* and *SOCS3 genes* (Table 2). Furthermore, APP/PS1 genetic background had a main effect on mRNA level of *Iba-1*.

3.5. The food-anticipation activity is impaired in HSD APP/PS1 mice

It has been suggested that the DMH modulates the wakefulness and food-anticipation activity of the food-entrainable circadian (Mieda et al., 2006; Tahara and Shibata, 2013). The attenuated leptin signaling in the DMH of HSD APP/PS1 mice prompted us to investigate whether the food anticipation activity of HSD APP/PS1 mice was altered after 23 weeks of dietary manipulation. The experimental design is shown in Fig 5A. During food-restricted training (RF), food pellets were provided from 11:00–15:00 in the light phase. After 9 days of RF, NF pellets were provided during the following day (NF). The distance traveled in 24 hours was measured on the ALF day, the 9th day of RF, and the NF day (Fig. 5B–D). Locomotion was induced before the feeding period on the 9th day of RF and the NF day (Fig. 5C and D). The total distances traveled by the 4 groups from 7:00 to 15:00 during the ALF day, the 9th day of RF, and the NF day were compared. The travel distance between the 4 groups was not different during the ALF day from 7:00 to 15:00 (Fig. 5E). On the 9th day of RF training, the travel distance of HSD groups from 7:00 to 15:00 was significantly lower than that of NCD groups, suggesting that the anticipatory activity of HSD groups was reduced (Fig. 5F). On the NF day, the distance traveled from 7:00 to 15:00 by HSD APP/PS1 mice was the lowest of the 4 groups, suggesting that the anticipatory activity related to food availability of HSD APP/PS1 mice was further attenuated compared with the other 3 groups (Fig. 5G). Statistically similar results were obtained for the distance traveled from 7:00 to 19:00 by the 4 groups during the ALF day, the 9th day of RF, and the NF day (Supplemental Fig. 5A–C).

The distance traveled in the critical time period spanning 2 hours before and 2 hours after the feeding time on the NF day was further analyzed. Consistently, the distance traveled by HSD APP/PS1 mice in the 4 time periods (9:00 to 10:00, 9:00 to 11:00, 9:00 to 12:00, and 9:00 to 13:00) was lower than that of NCD APP/PS1 mice on the NF day (Fig. 5H). However, no difference in the distance traveled between NCD WT and HSD WT mice was observed for any time period.

There was no difference in the locomotor activity during the dark cycle (19:00 to 7:00) between the 4 groups on the ALF, RF, and NF days, which suggests that the overall locomotor activity of the 4 groups was similar (Supplemental Fig. 5D–F). Consistently, the hourly locomotor activity during the dark cycle on the NF day was not significantly different between the 4 groups (Supplemental Fig. 5G). Therefore, the reduced travel distance of HSD APP/PS1 mice from 7:00 to 15:00 on the NF day was not due to a general attenuation of locomotor activity. Two-way ANOVA showed that HSD interacted with APP/PS1 genetic background for the travel distance on the NF day and that both HSD and APP/PS1 genetic background had simple main effects (Table 4).

3.6. HSD and APP/PS1 genetic background affect the ability to construct nests and burrow

In addition to an attenuation of locomotion on the RF and NF days by HSD APP/PS1 mice, motor activity, anxiety, and cognition behaviors were also evaluated to determine whether HSD altered the mobility, anxiety, and cognitive functions of APP/PS1 and WT mice at 26–27 weeks after dietary manipulation. The total movement distance, duration in the center zone, and the frequency of center crossing of 4 groups in the open field test were comparable, and the results suggested that the motor activity and anxiety of HSD groups were not different to those of NCD groups (Fig. 6A–C). The number of marbles buried by HSD WT mice was significantly lower than that of NCD WT mice, whereas the number of marbles buried by HSD APP/PS1 mice was not different from that of NCD APP/PS1 mice (Fig. 6D). The marble burying, one of anxiety measurements, revealed that anxiety level of HSD WT mice was lower than that of NCD WT mice, but that there was no difference for APP/PS1 groups.

Nesting and burrowing tasks were used to evaluate the impact of HSD and AD pathology on cognition and daily living capability. The nest score of NCD WT mice was higher than that of HSD WT mice; however, no difference was observed between that of NCD WT and NCD APP/PS1 mice. Furthermore, the nest score of HSD WT mice was not different from that of HSD APP/PS1 mice (Fig. 6E). The nest completion time of HSD APP/PS1 group was longer than that of HSD WT group (Fig. 6G). No differences between NCD and HSD APP/PS1 mice in the nest scores, unshredded Nestlet weight, and nest completion time, which suggests that the cognition of NCD APP/PS1 mice after 26–27 weeks of dietary manipulation (when the mice were 36–37 week old), was already impaired (Fig. 6E–G). The weight of food pellets burrowed by for HSD APP/PS1 mice was less than that of NCD APP/PS1 mice, which suggests that the daily living capability of APP/PS1 mice was hindered by HSD (Fig. 6H). Two-way ANOVA showed that HSD and APP/PS1 genetic background did not

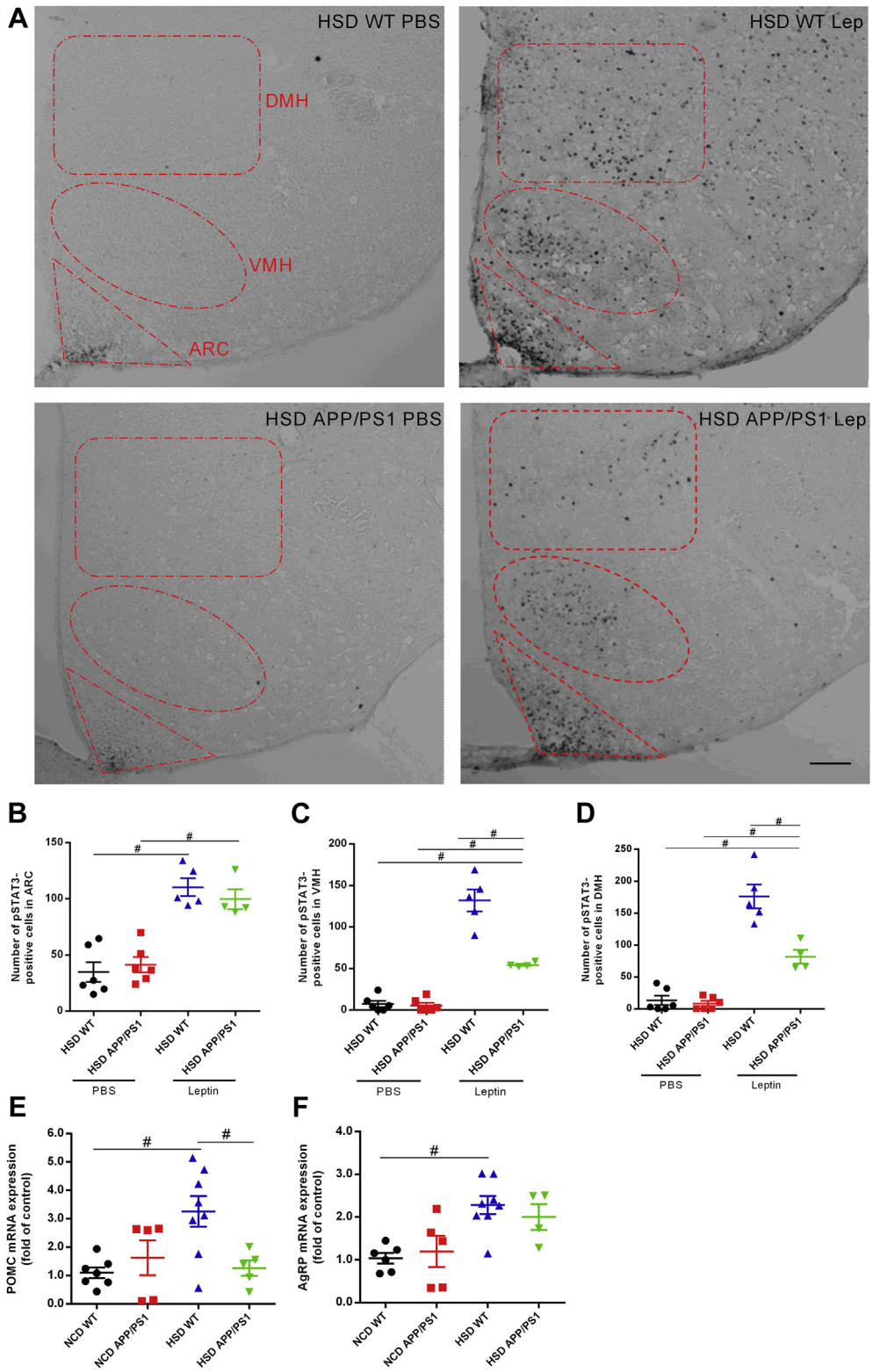

Fig. 4. HSD attenuated leptin-induced pSTAT3 expression in the DMH and VMH of APP/PS1 mice. (A) Representative images of pSTAT3-positive cells in the ARC, VMH, and DMH of HSD WT and APP/PS1 mice after the injection of leptin (Lep) or the vehicle (PBS) after 28 wk of dietary manipulation. The third ventricle is on the left of each panel. The red dotted lines define the areas of the ARC, VMH, and DMH for which the numbers of pSTAT3-positive cells were quantified after 28 wk of dietary manipulation. Scale bar represents 100 μm. (B–D) The numbers of pSTAT3-positive cells in the ARC, VMH, and DMH of HSD WT mice injected with PBS ($n = 6$), HSD WT mice injected with leptin ($n = 5$), HSD APP/PS1 mice injected with PBS ($n = 6$), and HSD APP/PS1 mice injected with leptin ($n = 4$) were quantified. (E) The mRNA expression levels of *POMC* gene in the hypothalamus of NCD WT mice ($n = 5$), NCD APP/PS1 mice ($n = 5$), HSD WT mice ($n = 8$), and HSD APP/PS1 mice ($n = 5$) were quantified by RT-PCR. (F) The mRNA expression levels of *AgRP* gene in the hypothalamus of NCD WT mice ($n = 5$), NCD APP/PS1 mice ($n = 5$), HSD WT mice ($n = 8$), and HSD APP/PS1 mice ($n = 4$) were quantified by RT-PCR. Data are expressed as mean ± SEM. Significant differences between groups were determined by one-way ANOVA followed by Bonferroni *post hoc* tests and are labeled using # ($p < 0.05$). Abbreviations: ANOVA, analysis of variance; ARC, arcuate nucleus; DMH, dorsomedial hypothalamus; HSD, high-sucrose diet; NCD, normal chow diet; pSTAT3, phosphorylated STAT3; VMH, ventromedial hypothalamus; WT, wild type. (For interpretation of the references to color in this figure legend, the reader is referred to the Web version of this article.)

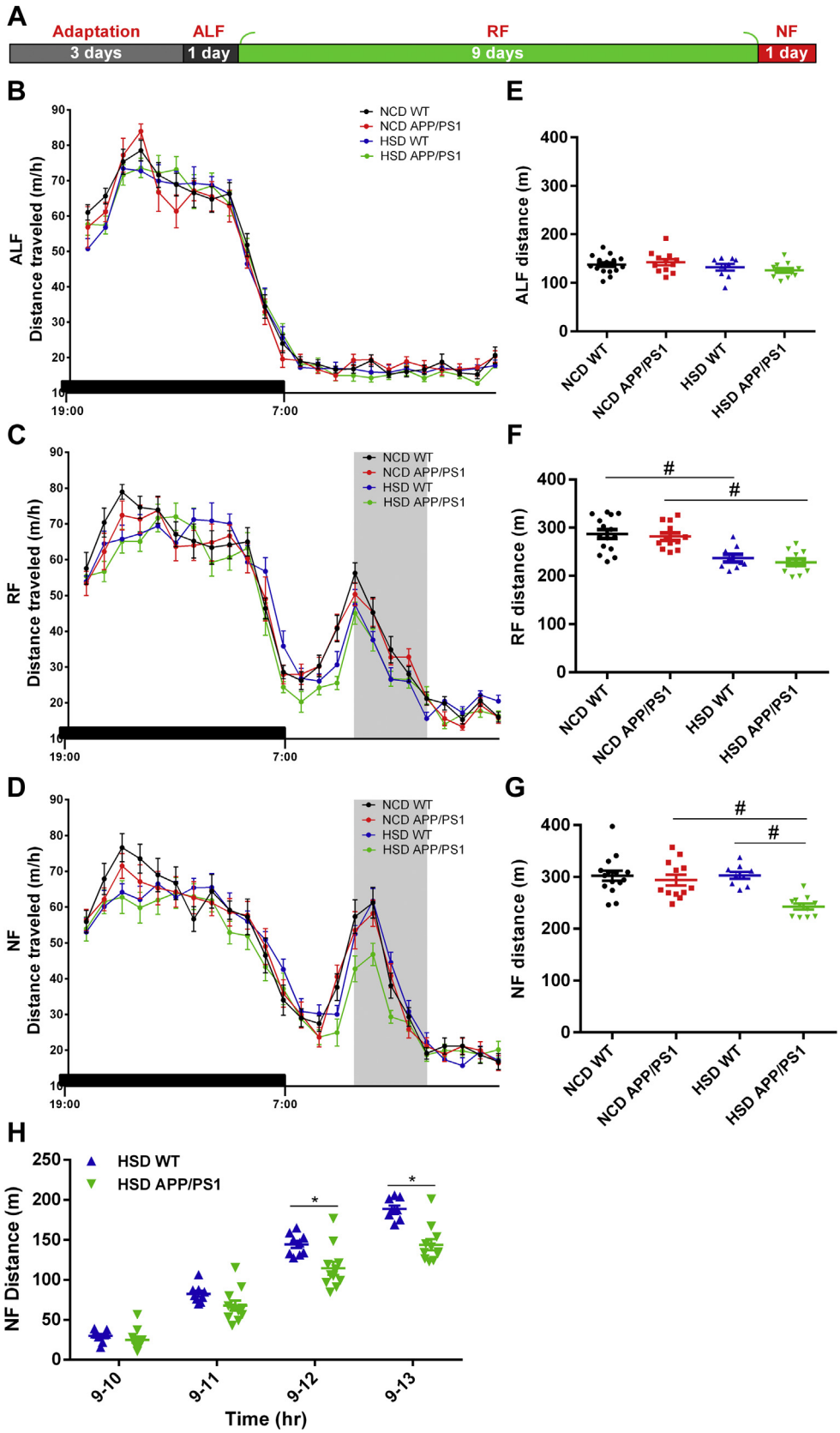

Fig. 5. HSD attenuated food-anticipatory activity of APP/PS1 mice. (A) Schematic diagram of the food entrainment test that was used to examine the food-entrainable circadian rhythms of NCD WT, NCD APP/PS1, HSD WT, and HSD APP/PS1 mice. After 23 wk of dietary manipulation, mice were recorded on the ALF day, the 9th day of RF, and NF day. (B–D) The distance traveled in 24 h during the day of ALF, the 9th day of RF, and the NF day by NCD WT mice ($n = 15$), NCD APP/PS1 mice ($n = 12$), HSD WT mice ($n = 9$), and HSD APP/PS1 mice ($n = 11$). The shaded period indicates that the feeding period spanned from 11:00 to 15:00 on the RF day (C) and that no food was given during this feeding period on the NF day (D). (E–G) The total distances traveled during 7:00–15:00 on the ALF day, the 9th day of RF, and the NF day by NCD WT mice ($n = 15$), NCD APP/PS1 mice ($n = 12$), HSD WT mice

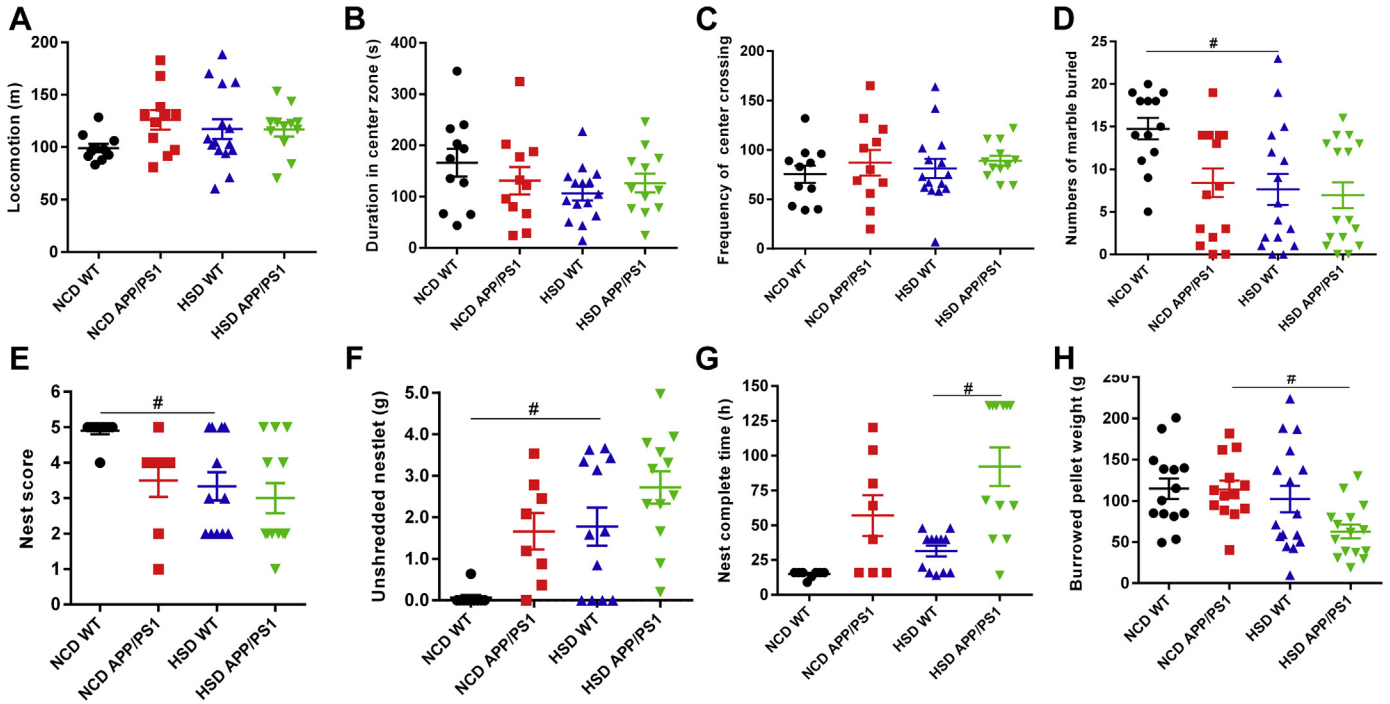

Fig. 6. HSD and APP/PS1 genetic background both affect nest construction and burrowing. The moving distance (A), duration in the center zone (B), and the frequency of center crossings (C) in the open field test of NCD WT mice ($n = 11$), NCD APP/PS1 mice ($n = 11$), HSD WT mice ($n = 15$), and HSD APP/PS1 mice ($n = 12$) were analyzed. (D) The numbers of marbles buried by NCD WT mice ($n = 13$), NCD APP/PS1 mice ($n = 15$), HSD WT mice ($n = 16$), and HSD APP/PS1 mice ($n = 16$) were compared. The nest score (E), weight of unshredded Nestlet (F), and the time for nest completion (G) by NCD WT mice ($n = 10$), NCD APP/PS1 mice ($n = 8$), HSD WT mice ($n = 12$), and HSD APP/PS1 mice ($n = 12$) were compared. (H) The weights of food pellets burrowed by NCD WT mice ($n = 14$), NCD APP/PS1 mice ($n = 13$), HSD WT mice ($n = 16$), and HSD APP/PS1 mice ($n = 15$) were compared. Data are expressed as the mean ± SEM. Significant differences between groups were determined by one-way ANOVA followed by Bonferroni *post hoc* tests and are labeled using # ($p < 0.05$). Abbreviations: ANOVA, analysis of variance; HSD, high-sucrose diet; NCD, normal chow diet; WT, wild type.

interact with each other but that both had a main effect on marble burying and nesting behaviors (Table 4).

4. Discussion

The impact of HSD on hypothalamus-mediated energy homeostasis has not been well studied compared with the effects of HFD; this is possibly because of the absence of obesity or the presence of only minor weight gains among the model animals (Flister et al., 2018). Furthermore, the hypothalamus-involved noncognitive symptoms of HSD APP/PS1 mice remain largely unexplored. Our findings suggest that HSD induces a mild weight gain and that there is exacerbation of glycemic dysregulation among APP/PS1 mice. We have further demonstrated that HSD attenuates leptin signaling in the DMH and VMH of APP/PS1 mice and alters their food-anticipatory activity. Our study is the first to suggest that HSD is able to differentially affect leptin signaling in the hypothalamic nuclei of APP/PS1 and WT mice.

The insulin resistance and increased Aβ burden of AD transgenic mice has been induced by sucrose-sweetened water (Cao et al., 2007; Orr et al., 2014). In this study, HSD solid food pellets were used to feed APP/PS1 mice and these contain relatively lower amounts of sucrose compared with the HSDs used to feed WT mice in previous studies. Our findings suggest that HSD interacts with APP/PS1 genetic background on the upregulation of GFAP and IL-1β and increases neuroinflammation. Furthermore, elevated serum IL-6, which can be released by enlarged visceral adipose tissue in HSD APP/PS1 mice, may also contribute to peripheral insulin resistance (Shie et al., 2015).

Both HSD-fed rodents and high fructose–fed rats have a higher body fat content and reduced leptin effectiveness (Bray, 2004; Harris, 2018; Oliveira et al., 2014). Only one report has shown that a high-fructose diet attenuated leptin-induced feeding suppression and hypothalamic pSTAT3 induction in WT rats; however, pSTAT3 activity in individual hypothalamic nuclei was not investigated (Shapiro et al., 2008). Our work is the first to demonstrate that HSD APP/PS1 mice had attenuated leptin-induced pSTAT3 in the VMH and DMH but not in the ARC.

In our previous study, we compared the number of leptin-induced pSTAT3-positive cells in NCD WT and NCD APP/PS1 mice (Lee et al., 2018). The results showed that leptin-induced pSTAT3 expression was similar in the ARCs, VMHs, or DMHs of NCD WT and APP/PS1 mice. In the present study, our results indicate that leptin-induced pSTAT3 expression is significantly lower in the VMH and DMH but not in the ARC of HSD APP/PS1 mice than of HSD WT mice. Two-way ANOVA showed that the decrease in leptin-induced pSTAT3 in HSD APP/PS1 mice versus HSD WT mice is due to the interaction of APP/PS1 genetic background and HSD.

In addition to roles in energy homeostasis, the DMH is involved in modulating food-entrainable circadian rhythms, and the VMH is

($n = 9$), and HSD APP/PS1 mice ($n = 11$) were compared. (H) The distances traveled during 9:00–10:00, 9:00–11:00, 9:00–12:00, and 9:00–13:00 periods by NCD WT mice ($n = 15$), NCD APP/PS1 mice ($n = 12$), HSD WT mice ($n = 9$), and HSD APP/PS1 mice ($n = 11$) were compared on the NF day. (E–G) Data are expressed as mean ± SEM. Statistical differences between groups were determined by one-way ANOVA followed by Bonferroni *post hoc* tests and are labeled using # ($p < 0.05$). (H) The distances traveled during 9:00–10:00, 9:00–11:00, 9:00–12:00, and 9:00–13:00 periods by NCD WT mice ($n = 15$), NCD APP/PS1 mice ($n = 12$), HSD WT mice ($n = 9$), and HSD APP/PS1 mice ($n = 11$) were compared on the NF day. Data are expressed as mean ± SEM. Statistical differences between groups were determined by an unpaired Student's *t*-test and labeled using * ($p < 0.05$). Abbreviations: ANOVA, analysis of variance; ALF, *ad libitum* feeding; HSD, high-sucrose diet; NCD, normal chow diet; NF, no food; RF, restricted feeding; WT, wild type.

essential for systemic glycemic regulation (Gooley et al., 2006; Shimazu and Minokoshi, 2017). The glycemic dysregulation observed in HSD APP/PS1 mice during our study may be associated with reduced leptin signaling in the VMH. The DMH is required to anticipate the feeding times of wake-sleep and locomotion during RF (Saper, 2013). Food anticipation was found to be normal for NCD APP/PS1 mice, which is consistent with the previous study during which food anticipation was normal for APP/PS1 mice fed regular chow (Kent et al., 2019). We report here that HSD APP/PS1 mice show altered food-entrainable circadian rhythms that may contribute to the noncognitive symptoms of AD. This altered feeding behavior may be associated with an attenuation of leptin signaling in the DMH. However, the involvement of the DMH in food-anticipatory activity remains controversial (Landry et al., 2006, 2007, 2011; Moriya et al., 2009). In addition, 2 studies have shown that a loss of leptin signaling is associated with increased food anticipation in rat and mice (Mistlberger and Marchant, 1999; Ribeiro et al., 2011). Therefore, it is possible that the HSD alterations in the food-entrainable circadian rhythms of APP/PS1 mice may be mediated by other pathways with or without the involvement of attenuated leptin signaling in the DMH.

The major difference between food-anticipatory activity on the day 9 of RF and the NF day is that a decrease in food-anticipatory activity was found for HSD WT mice compared with NCD WT mice on the 9th day of RF, but this was not the case for the NF day. One interpretation of this result is that there is HSD-impaired food-anticipatory activity in both WT and APP/PS1 mice but that the memory of food-entrained behavior is impaired in HSD APP/PS1 mice, but not in HSD WT mice.

Although senile plaques and mRNA upregulation of *GFAP* and *Iba-1* genes were not detected in the hypothalamus, elevated neuroinflammation in the cortex and hippocampus of HSD APP/PS1 mice may have had an effect on hypothalamic functioning via the interconnected limbic system (Lee et al., 2018; Yeh et al., 2015). A recent study has indicated that an increase in stalled blood flow in the cortical capillaries of APP/PS1 and 5×FAD mice relative to WT mice brings about an impairment of memory functions (Cruz Hernandez et al., 2019). Therefore, AD-related pathology in the cortex and hippocampus is likely to hinder neuronal functioning via the limbic system.

Upregulation of *NPY* and downregulation of *POMC* have been observed previously in HFD-induced obesity groups compared with diet-resistant groups (Cifani et al., 2015). Furthermore, the transcriptional regulation of *NPY* and *POMC* genes is inversely correlated with DNA methylation of the promoter regions of *NPY* and *POMC* genes of the HFD-induced obesity groups. In the present study, the mRNA levels of *AgRP and POMC* genes were found to be upregulated in the hypothalamus of HSD WT mice, but this was not the case for HSD APP/PS1 mice. In our previous study, hyperphagia was found to be induced in the first 2 days after the dietary switch and after 23 weeks on HFD (Lee et al., 2018). In contrast, hyperphagia was not induced by HSD in the present study. Up to the present, no study has revealed an effect of HSD on the mRNA expression of *NPY* and *POMC* genes in the hypothalamus, and therefore, the impact of the changes in the expression profiles of *AgRP* and *POMC* genes in response to HSD on the energy homeostasis of WT and APP/PS1 mice is not clear.

The role of hypothalamic microglial activation in HFD-induced obesity is well established (Valdearcos et al., 2018). However, whether HSD induces the activation of hypothalamic microglia remains unstudied. Using a diet containing high sucrose and high fat, Gao et al. have shown that microgliosis and astrogliosis in the ARC are enhanced (Gao et al., 2017). In their study, hypothalamic neuroinflammation was induced by the interaction between a high fat content and a high sucrose content. Nevertheless, we did not observe any difference in the expression of Iba-1 and GFAP in the hypothalamus of the 4 groups. The fat content of HSD used in our study is comparable to that found in NCD we used. Therefore, the discrepancy between our results and theirs may be due to the significant difference in fat content between the diets and the difference in treatment durations.

In conclusion, high sucrose consumption from solid pellets accelerates insulin intolerance, induces feeding behavior abnormalities, increases cortical and serum levels of Aβ, and causes inflammation within the CNS and peripheral systems of APP/PS1 mice. Our findings indicate that HSD induced minor weight gain, exacerbated glycemic dysregulation, attenuated leptin signaling in the DMH and VMH of APP/PS1 mice, and altered food-entrainable circadian rhythms during NF. Our study is the first to suggest that HSD differentially affects leptin signaling in the hypothalamic nuclei of APP/PS1 and WT mice. This attenuation of leptin signaling in HSD APP/PS1 mice may be correlated with increased Aβ levels, an elevation of neuroinflammation, and increased noncognitive impairment in AD.

Disclosure

No authors have any actual or potential conflicts of interest, including any financial, personal, or other relationships with other people or organizations within 3 years of beginning this work that could inappropriately influence the work.

Acknowledgements

The authors thank Dr Shi-Bing Yang, Chih-Wen Yeh, Hao-Chieh Hsu, Hui-Wen Chen, and Meng-An Chien for their help with analyzing the data of pSTAT3, leptin inhibition of feeding, and the food entrainment test. This project was supported by the Ministry of Science and Technology in Taiwan, MOST105-2320-B-010-021, 106–2320-B010-022, 106-2314-B-010-012-MY3, and 106–2320-B-077-MY3. It was also supported by the National Health Research Institutes (NP-PP03) and Central Government S&T grant, Taiwan (NPGP07-034). In addition, it was supported by the Brain Research Center of National Yang-Ming University from The Featured Areas Research Center Program within the framework of the Higher Education Sprout Project by the Ministry of Education (MOE) in Taiwan.

Author Contributions: Investigation was done by Skye Hsin-Hsien Yeh, Feng-Shiun Shie, Hui-Kang Liu, Li-Min Chen, and Kuan-Wei Wu. Data analysis was conducted by Heng-Hsiang Yao, Yi-Heng Lee, Pei-Chen Kao, Shu-Meng Hsu, and Li-Jung Chao. Project administration was carried out by Huey-Jen Tsay. Resources were provided by Skye Hsin-Hsien Yeh and Feng-Shiun Shie. Supervision was done by Young-Ji Shiao and Huey-Jen Tsay. Writing—original draft was carried out by Huey-Jen Tsay. Writing—review & editing was carried out by Young-Ji Shiao and Huey-Jen Tsay.

Appendix A. Supplementary data

Supplementary data associated with this article can be found, in the online version, at https://doi.org/10.1016/j.neurobiolaging.2019.11.018.

References

Adebakin, A., Bradley, J., Gumusgoz, S., Waters, E.J., Lawrence, C.B., 2012. Impaired satiation and increased feeding behaviour in the triple-transgenic Alzheimer's disease mouse model. PLoS One 7, e45179.

Apolzan, J.W., Harris, R.B.S., 2013. Rapid onset and reversal of peripheral and central leptin resistance in rats offered chow, sucrose solution, and lard. Appetite 60, 65–73.

Baglietto-Vargas, D., Shi, J., Yaeger, D.M., Ager, R., LaFerla, F.M., 2016. Diabetes and Alzheimer's disease crosstalk. Neurosci. Biobehav. Rev. 64, 272–287.

Ballestri, S., Nascimbeni, F., Baldelli, E., Marrazzo, A., Romagnoli, D., Lonardo, A., 2017. NAFLD as a sexual dimorphic disease: role of gender and reproductive

status in the development and progression of nonalcoholic fatty liver disease and inherent cardiovascular risk. Adv. Ther. 34, 1291–1326.
Bomfim, T.R., Forny-Germano, L., Sathler, L.B., Brito-Moreira, J., Houzel, J.C., Decker, H., Silverman, M.A., Kazi, H., Melo, H.M., McClean, P.L., Holscher, C., Arnold, S.E., Talbot, K., Klein, W.L., Munoz, D.P., Ferreira, S.T., De Felice, F.G., 2012. An anti-diabetes agent protects the mouse brain from defective insulin signaling caused by Alzheimer's disease- associated Abeta oligomers. J. Clin. Invest. 122, 1339–1353.
Bonda, D.J., Stone, J.G., Torres, S.L., Siedlak, S.L., Perry, G., Kryscio, R., Jicha, G., Casadesus, G., Smith, M.A., Zhu, X., Lee, H.G., 2014. Dysregulation of leptin signaling in Alzheimer disease: evidence for neuronal leptin resistance. J. Neurochem. 128, 162–172.
Bray, G.A., 2004. The epidemic of obesity and changes in food intake: the fluoride hypothesis. Physiol. Behav. 82, 115–121.
Bray, G.A., Nielsen, S.J., Popkin, B.M., 2004. Consumption of high-fructose corn syrup in beverages may play a role in the epidemic of obesity. Am. J. Clin. Nutr. 79, 537–543.
Burgeiro, A., Cerqueira, M.G., Varela-Rodriguez, B.M., Nunes, S., Neto, P., Pereira, F.C., Reis, F., Carvalho, E., 2017. Glucose and lipid dysmetabolism in a rat model of prediabetes induced by a high-sucrose diet. Nutrients 9, 638.
Cao, D., Lu, H., Lewis, T.L., Li, L., 2007. Intake of sucrose-sweetened water induces insulin resistance and exacerbates memory deficits and amyloidosis in a transgenic mouse model of Alzheimer disease. J. Biol. Chem. 282, 36275–36282.
Caron, A., Lee, S., Elmquist, J.K., Gautron, L., 2018. Leptin and brain-adipose cross-talks. Nat. Rev. Neurosci. 19, 153–165.
Cifani, C., Micioni Di Bonaventura, M.V., Pucci, M., Giusepponi, M.E., Romano, A., Di Francesco, A., Maccarrone, M., D'Addario, C., 2015. Regulation of hypothalamic neuropeptides gene expression in diet induced obesity resistant rats: possible targets for obesity prediction? Front. Neurosci. 9, 187.
Cruz Hernandez, J.C., Bracko, O., Kersbergen, C.J., 2019. Neutrophil adhesion in brain capillaries reduces cortical blood flow and impairs memory function in Alzheimer's disease mouse models. Nat. Neurosci. 22 (3), 413–420.
De Felice, F.G., Lourenco, M.V., Ferreira, S.T., 2014. How does brain insulin resistance develop in Alzheimer's disease? Alzheimers Dement. 10 (1 Suppl), S26–S32.
de la Monte, S.M., 2017. Insulin resistance and neurodegeneration: progress towards the development of new therapeutics for Alzheimer's disease. Drugs 77, 47–65.
Deacon, R.M., 2006. Assessing nest building in mice. Nat. Protoc. 1, 1117–1119.
Do, K., Laing, B.T., Landry, T., Bunner, W., Mersaud, N., Matsubara, T., Li, P., Yuan, Y., Lu, Q., Huang, H., 2018. The effects of exercise on hypothalamic neurodegeneration of Alzheimer's disease mouse model. PLoS One 13, e0190205.
Flister, K.F.T., Pinto, B.A.S., Franca, L.M., Coelho, C.F.F., Dos Santos, P.C., Vale, C.C., Kajihara, D., Debbas, V., Laurindo, F.R.M., Paes, A.M.A., 2018. Long-term exposure to high-sucrose diet down-regulates hepatic endoplasmic reticulum-stress adaptive pathways and potentiates de novo lipogenesis in weaned male mice. J. Nutr. Biochem. 62, 155–166.
Frazier, H.N., Ghoweri, A.O., Anderson, K.L., Lin, R.L., Porter, N.M., Thibault, O., 2019. Broadening the definition of brain insulin resistance in aging and Alzheimer's disease. Exp. Neurol. 313, 79–87.
Gao, Y., Bielohuby, M., Fleming, T., Grabner, G.F., Foppen, E., Bernhard, W., Guzman-Ruiz, M., Layritz, C., Legutko, B., Zinser, E., Garcia-Caceres, C., Buijs, R.M., Woods, S.C., Kalsbeek, A., Seeley, R.J., Nawroth, P.P., Bidlingmaier, M., Tschop, M.H., Yi, C.X., 2017. Dietary sugars, not lipids, drive hypothalamic inflammation. Mol. Metab. 6, 897–908.
Gooley, J.J., Schomer, A., Saper, C.B., 2006. The dorsomedial hypothalamic nucleus is critical for the expression of food-entrainable circadian rhythms. Nat. Neurosci. 9, 398–407.
Hannou, S.A., Haslam, D.E., McKeown, N.M., Herman, M.A., 2018. Fructose metabolism and metabolic disease. J. Clin. Invest. 128, 545–555.
Harris, R.B.S., 2018. Source of dietary sucrose influences development of leptin resistance in male and female rats. Am. J. Physiol. Regul. Integr. Comp. Physiol. 314, R598–R610.
Heneka, M.T., Carson, M.J., El Khoury, J., Landreth, G.E., Brosseron, F., Feinstein, D.L., Jacobs, A.H., Wyss-Coray, T., Vitorica, J., Ransohoff, R.M., Herrup, K., Frautschy, S.A., Finsen, B., Brown, G.C., Verkhratsky, A., Yamanaka, K., Koistinaho, J., Latz, E., Halle, A., Petzold, G.C., Town, T., Morgan, D., Shinohara, M.L., Perry, V.H., Holmes, C., Bazan, N.G., Brooks, D.J., Hunot, S., Joseph, B., Deigendesch, N., Garaschuk, O., Boddeke, E., Dinarello, C.A., Breitner, J.C., Cole, G.M., Golenbock, D.T., Kummer, M.P., 2015. Neuroinflammation in Alzheimer's disease. Lancet Neurol. 14, 388–405.
Hiller, A.J., Ishii, M., 2018. Disorders of body weight, sleep and circadian rhythm as manifestations of hypothalamic dysfunction in Alzheimer's disease. Front. Cell. Neurosci. 12, 471.
Ishii, M., Iadecola, C., 2015. Metabolic and non-cognitive manifestations of Alzheimer's disease: the hypothalamus as both culprit and target of pathology. Cell Metab. 22, 761–776.
Kent, B.A., Michalik, M., Marchant, E.G., Yau, K.W., Feldman, H.H., Mistlberger, R.E., Nygaard, H.B., 2019. Delayed daily activity and reduced NREM slow-wave power in the APPswe/PS1dE9 mouse model of Alzheimer's disease. Neurobiol. Aging 78, 74–86.
Kim, D.W., Glendining, K.A., Grattan, D.R., Jasoni, C.L., 2016. Maternal obesity leads to increased proliferation and numbers of astrocytes in the developing fetal and neonatal mouse hypothalamus. Int. J. Dev. Neurosci. 53, 18–25.
Knights, A.J., Funnell, A.P., Pearson, R.C., Crossley, M., Bell-Anderson, K.S., 2014. Adipokines and insulin action a sensitive issue. Adipocyte 3, 88–96.
Landry, G.J., Simon, M.M., Webb, I.C., Mistlberger, R.E., 2006. Persistence of a behavioral food-anticipatory circadian rhythm following dorsomedial hypothalamic ablation in rats. Am. J. Physiol. Regul. Integr. Comp. Physiol. 290, R1527–R1534.
Landry, G.J., Kent, B.A., Patton, D.F., Jaholkowski, M., Marchant, E.G., Mistlberger, R.E., 2011. Evidence for time-of-day dependent effect of neurotoxic dorsomedial hypothalamic lesions on food anticipatory circadian rhythms in rats. PLoS One 6, e24187.
Landry, G.J., Yamakawa, G.R., Webb, I.C., Mear, R.J., Mistlberger, R.E., 2007. The dorsomedial hypothalamic nucleus is not necessary for the expression of circadian food-anticipatory activity in rats. J. Biol. Rhythms 22, 467–478.
Lee, Y.H., Hsu, H.C., Kao, P.C., 2018. Augmented insulin and leptin resistance of high fat diet-fed APPswe/PS1dE9 transgenic mice exacerbate obesity and glycemic dysregulation. Int. J. Mol. Sci. 19, 2333.
Lyra e Silva, N.M., Goncalves, R.A., Boehnke, S.E., Forny-Germano, L., Munoz, D.P., De Felice, F.G., 2019. Understanding the link between insulin resistance and Alzheimer's disease: insights from animal models. Exp. Neurol. 316, 1–11.
Malik, V.S., Popkin, B.M., Bray, G.A., Despres, J.P., Hu, F.B., 2010. Sugar-sweetened beverages, obesity, type 2 diabetes mellitus, and cardiovascular disease risk. Circulation 121, 1356–1364.
Masters, C.L., Bateman, R., Blennow, K., Rowe, C.C., Sperling, R.A., Cummings, J.L., 2015. Alzheimer's disease. Nat. Rev. Dis. Primers 1, 15056.
Mieda, M., Williams, S.C., Richardson, J.A., Tanaka, K., Yanagisawa, M., 2006. The dorsomedial hypothalamic nucleus as a putative food-entrainable circadian pacemaker. Proc. Natl. Acad. Sci. U. S. A. 103, 12150–12155.
Mistlberger, R.E., Marchant, E.G., 1999. Enhanced food-anticipatory circadian rhythms in the genetically obese Zucker rat. Physiol. Behav. 66, 329–335.
Moriya, T., Aida, R., Kudo, T., et al., 2009. The dorsomedial hypothalamic nucleus is not necessary for food-anticipatory circadian rhythms of behavior, temperature or clock gene expression in mice. Eur. J. Neurosci. 29, 1447–1460.
Mortera, R.R., Bains, Y., Gugliucci, A., 2019. Fructose at the crossroads of the metabolic syndrome and obesity epidemics. Front. Biosci. (Landmark Ed) 24, 186–211.
Oliveira, L.S., Santos, D.A., Barbosa-da-Silva, S., Mandarim-de-Lacerda, C.A., Aguila, M.B., 2014. The inflammatory profile and liver damage of a sucrose-rich diet in mice. J. Nutr. Biochem. 25, 193–200.
Orr, M.E., Salinas, A., Buffenstein, R., Oddo, S., 2014. Mammalian target of rapamycin hyperactivity mediates the detrimental effects of a high sucrose diet on Alzheimer's disease pathology. Neurobiol. Aging 35, 1233–1242.
Pape, J.A., Newey, C.R., Burrell, H.R., Workman, A., 2018. Per-arnt-sim Kinase (PASK) deficiency increases cellular respiration on a standard diet and decreases liver triglyceride accumulation on a western high-fat high-sugar diet. Nutrients 10 (12), 1–16.
Ribeiro, A.C., Ceccarini, G., Dupré, C., Friedman, J.M., Pfaff, D.W., Mark, A.L., 2011. Contrasting effects of leptin on food anticipatory and total locomotor activity. PLoS One 6, e23364.
Sakono, M., Zako, T., 2010. Amyloid oligomers: formation and toxicity of Abeta oligomers. FEBS J. 277, 1348–1358.
Saper, C.B., 2013. The central circadian timing system. Curr. Opin. Neurobiol. 23, 747–751.
Schultz, A., Barbosa-da-Silva, S., Aguila, M.B., Mandarim-de-Lacerda, C.A., 2015. Differences and similarities in hepatic lipogenesis, gluconeogenesis and oxidative imbalance in mice fed diets rich in fructose or sucrose. Food Funct. 6, 1684–1691.
Schulz, L.C., Widmaier, E.P., 2006. Leptin receptors. In: Henson, M.C., Castracane, V.D. (Eds.), Leptin Endocrinology Update Series. Springer Publishing Co, New York.
Seshadri, S., Rapaka, N., Prajapati, B., Mandaliya, D., Patel, S., Muggalla, C.S., Kapadia, B., 2019. Statins exacerbate glucose intolerance and hyperglycemia in a high sucrose fed rodent model. Sci. Rep. 9 (1), 8825.
Shapiro, A., Mu, W., Roncal, C., Cheng, K.-Y., Johnson, R.J., Scarpace, P.J., 2008. Fructose-induced leptin resistance exacerbates weight gain in response to subsequent high-fat feeding. Am. J. Physiol. Regul. Integr. Comp. Physiol. 295, R1370–R1375.
Shie, F.S., Shiao, Y.J., Yeh, C.W., Lin, C.H., Tzeng, T.T., Hsu, H.C., Huang, F.L., Tsay, H.J., Liu, H.K., 2015. Obesity and hepatic steatosis are associated with elevated serum amyloid beta in metabolically stressed APPswe/PS1dE9 mice. PLoS One 10, e0134531.
Shimazu, T., Minokoshi, Y., 2017. Systemic glucoregulation by glucose-sensing neurons in the ventromedial hypothalamic nucleus (VMH). J. Endocr. Soc. 1, 449–459.
Spielman, L.J., Little, J.P., Klegeris, A., 2014. Inflammation and insulin/IGF-1 resistance as the possible link between obesity and neurodegeneration. J. Neuroimmunol. 273, 8–21.
Tahara, Y., Shibata, S., 2013. Chronobiology and nutrition. Neuroscience 253, 78–88.
Thomas, A., Burant, A., Bui, N., Graham, D., Yuva-Paylor, L.A., Paylor, R., 2009. Marble burying reflects a repetitive and perseverative behavior more than novelty-induced anxiety. Psychopharmacology 204, 361–373.
Tillman, E.J., Morgan, D.A., Rahmouni, K., Swoap, S.J., 2014. Three months of high-fructose feeding fails to induce excessive weight gain or leptin resistance in mice. PLoS One 9, e107206.
Tzeng, T.T., Chen, C.C., Chen, C.C., Tsay, H.J., Lee, L.Y., Chen, W.P., Shen, C.C., 2018. The cyanthin diterpenoid and sesterterpene constituents of Hericium erinaceus mycelium Ameliorate Alzheimer's disease-related pathologies in APP/PS1 transgenic mice. Int. J. Mol. Sci. 19 (2), 589.

Valdearcos, M., Douglass, J.D., Robblee, M.M., Dorfman, M.D., Stifler, D.R., Bennett, M.L., Gerritse, I., Fasnacht, R., Barres, B.A., Thaler, J.P., Koliwad, S.K., 2018. Microglial inflammatory signaling orchestrates the hypothalamic immune response to dietary excess and mediates obesity susceptibility. Cell Metab. 27, 1356.

van Swieten, M.M., Pandit, R., Adan, R.A., van der Plasse, G., 2014. The neuroanatomical function of leptin in the hypothalamus. J. Chem. Neuroanat. 61-62, 207–220.

Yeh, C.W., Yeh, S.H., Shie, F.S., Lai, W.S., Liu, H.K., Tzeng, T.T., Tsay, H.J., Shiao, Y.J., 2015. Impaired cognition and cerebral glucose regulation are associated with astrocyte activation in the parenchyma of metabolically stressed APPswe/PS1dE9 mice. Neurobiol. Aging 36, 2984–2994.

Zhang, Y., Zhou, B., Deng, B., Zhang, F., Wu, J., Wang, Y., Le, Y., Zhai, Q., 2013. Amyloid-beta induces hepatic insulin resistance in vivo via JAK2. Diabetes 62, 1159–1166.

Zhang, Z.Y., Dodd, G.T., Tiganis, T., 2015. Protein tyrosine phosphatases in hypothalamic insulin and leptin signaling. Trends Pharmacol. Sci. 36, 661–674.